A WEAP-MODFLOW surface water-groundwater model for the irrigated Miyandoab plain, Urmia lake basin, Iran
Multi-objective calibration and quantification of historical drought impacts

Dehghanipour, Amir Hossein; Zahabiyoun, Bagher; Schoups, Gerrit; Babazadeh, Hossein

Important note
To cite this publication, please use the final published version (if applicable).
Please check the document version above.

A WEAP-MODFLOW surface water-groundwater model for the irrigated Miyandoab plain, Urmia lake basin, Iran: Multi-objective calibration and quantification of historical drought impacts

Amir Hossein Dehghanipour[a,*], Bagher Zahabiyoun[a], Gerrit Schoups[b], Hossein Babazadeh[c]

[a] Department of Water Management, School of Civil Engineering, Iran University of Science and Technology, Tehran, Iran

[b] Department of Water Management, Faculty of Civil Engineering and Geosciences, Delft University of Technology, Delft, The Netherlands

[c] Department of Water Science and Engineering, Science and Research Branch, Islamic Azad University, Tehran, Iran

Abstract

This study develops and applies the first coupled surface water-groundwater (SW-GW) flow model for the irrigated Miyandoab plain located in the Urmia basin, in the northwest of Iran. The model is implemented using a dynamic coupling between MODFLOW and WEAP and consists of spatially distributed monthly water balances for the aquifer, root-zone, rivers, canals, and reservoirs. Multi-objective calibration of the model using river discharge and GW level data yields accurate simulation of historical conditions, and results in better constrained parameters compared to using either data source alone. Model simulations show that crop water demand cannot be met during droughts due to limited GW pumping capacity, and that increased GW pumping has a relatively strong impact on GW levels due to the small specific yield of the aquifer. The SW-GW model provides a unique tool for exploring management options that sustain agricultural production and downstream flow to the shrinking Urmia Lake.

Keywords: Urmia lake basin; Surface water-groundwater; WEAP; MODFLOW; Soil moisture method; Multi-objective calibration.

1. Introduction

In arid and semi-arid agricultural regions, irrigation is under pressure by decreasing water resources (Mancosu et al., 2015). Conjunctive use of surface water (SW) and groundwater (GW) resources can be a good strategy for dealing with decreases in water resources and for preventing loss of farming profits (Schoups et al., 2006). In addition, conjunctive use improves water use efficiency and reduces risks associated with uncertain SW supplies subject to climate variability (Paydar and Qureshi, 2012; Singh, 2014a). Researchers considered SW and GW resources as separate until the 1960s (Singh, 2014b). Buras (1963) presented one of the first studies in conjunctive use modeling and proposed that SW and GW should be considered as elements of a coupled water system. Several studies were performed to evaluate conjunctive use of SW and GW and improve water management in irrigated areas (e.g. Rogers and Smith, 1970; Chávez-Morales et al., 1992; Schoups et al., 2006; Montazar et al., 2010; Safavi and Esmikhani, 2013).

In many conjunctive use studies, SW-GW interactions were treated in a simplified manner (Safavi and Esmikhani, 2013). In conjunctive use management, it is very important to understand the interaction between GW and SW, and coupled SW-GW models are needed to accurately simulate the complex behavior of the integrated SW-GW system (Tian et al., 2015). In recent years, a number of coupled SW-GW models have been developed. MODSIM and

---

MODFLOW (Harbaugh, 2005) were linked to support conjunctive management of SW and GW (Fredericks et al., 1998). The SWATMOD model combines the Soil Water Assessment Tool (SWAT) (Arnold et al., 1998) and MODFLOW for simulating SW-GW interactions (Sophocleous et al., 1999). To improve the simulation of water surface profiles in open channels, MODFLOW and HEC-RAS have also been coupled (Rodriguez et al., 2008). The GSFLOW model combines the Precipitation-Runoff Modeling System (PRMS) (Leavesley et al., 1983) with MODFLOW (Huntington and Niswonger, 2012; Markstrom et al., 2008), while GSFLOW-SWMM in turn extends GSFLOW with the Storm Water Management Model (SWMM) (Rossman, 2004) for simulating SW diversions and GW pumping in irrigated areas (Tian et al., 2015). Finally, coupling of SWAT, MODFLOW and MT3DMS (Zheng and Wang, 1999) has also been reported (Ehtiat et al., 2018).

An important gap in the above-mentioned simulation tools is that they have limited capability for integrated water resources planning and scenarios analysis. Moreover, hydraulic structures (i.e. irrigation and drainage network) and their operations in irrigated areas are typically not supported (Tian et al., 2015). The Water Evaluation and Planning system (WEAP) was developed by the Stockholm Environment Institute in 1988 for integrated water resources planning. This modeling tool is used for planning as well as policy analysis and presenting solutions under long-term scenarios (Sieber and Purkey, 2015). The first application of WEAP concerned impacts of management strategies in the Aral Sea Basin (Raskina et al., 1992). WEAP has been widely used to study different integrated water resources planning issues in irrigated areas (e.g. Yates et al., 2005; Höllermann et al., 2010; Rousta and Araghinejad, 2015).

While WEAP's built-in GW modeling capabilities are limited, WEAP can also be linked to MODFLOW for simulating complex cases (Sieber and Purkey, 2015). Using coupled WEAP and MODFLOW models, Droubi et al. (2008) developed a Decision Support System (DSS) and applied it in the Zabadani basin, Syria. This study evaluated the developed DSS considering the impacts of climate change and changes in demand and supply on water availability. Le Page et al. (2012) presented a DSS using WEAP-MODFLOW and applied it to a semi-arid aquifer in Morocco. Hadded et al. (2013) developed a DSS for GW management of the 'Zeuss Koutine' aquifer in Tunisia using WEAP-MODFLOW. The developed DSS was used to evaluate the potential of a seawater desalination plant for reducing GW drawdowns. Nouiri et al. (2015) improved WEAP-MODFLOW by including a multi-objective optimization tool based on a Multi-Objective Genetic Algorithm. Objective functions consisted of satisfaction of demand, minimization of water cost, and maximization of GW withdrawal subject to water salinity constraints. The developed software was applied to a hypothetic aquifer as a case study. Sala et al. (2015) developed a coupled WEAP-MODFLW model for the Orontes River Basin in Lebanon. In this study, the MABIA method was used for the daily simulation of crop irrigation and a coupled WEAP-MODFLOW model was applied to investigate different water consumption scenarios to respond to situations of water stress.

There are two important gaps in studies that use coupled WEAP–MODFLOW models. First, to calibrate SW-GW models like WEAP-MODFLOW, one needs to find model parameter values that match multiple types of observations (typically, streamflow and aquifer head data). While manual trial-and-error can be used for this purpose, automated multi-objective calibration provides a more accurate and less time-consuming approach (e.g., Schoups et al., 2005; Tang et al., 2006; Moussa and Chahinian, 2009; Afshar et al., 2013). Second, overly simplistic methods are typically used for calculating GW recharge in WEAP-MODFLOW models. WEAP does include a more sophisticated approach known as the "soil moisture method", but it has not been used in coupled

WEAP-MODFLOW applications, even though it has been shown to be an efficient approach for calculating GW recharge in various WEAP applications that do not use MODFLOW (e.g. Yates et al., 2005; Alizadeh and Mousavi, 2013; Ingol-Blanco and McKinney, 2012).

The central goal of our work is to develop and apply a hydrological model for conjunctive management of SW and GW resources in the irrigated Miyandoab plain, a strategic agricultural region in the Urmia Basin in the semi-arid northwest of Iran. The hydrology of this plain is significantly impacted by irrigation activities, including SW withdrawals, irrigation recharge, and GW pumping, resulting in interactions between the SW, GW, and root-zone components of the system. GW heads in the region have dropped over time due to a reduction in precipitation as well as an increase in GW withdrawals for agricultural purposes. Moreover, environmental flows into Urmia lake, located just downstream of the irrigated plain, are not satisfied due to a combination of SW withdrawals for irrigation and climate change. To properly account for SW-GW interactions, our model is implemented using WEAP-MODFLOW, with MODFLOW simulating GW response and WEAP simulating SW and root-zone components of the system. Our study makes the following contributions in methodology and application:

1) we present the first coupled SW-GW hydrologic model for the Miyandoab Plain. Previous hydrologic models for this region (Ahmadzadeh et al., 2016; Hesami and Amini, 2016; Mohammadpour and Bagheri, 2017; Tehrani et al., 2012) have not coupled the SW and GW components of the system, 2) Compared to previous long-term WEAP-MODFLOW studies, a more sophisticated monthly root-zone water balance model (i.e. WEAP's "soil moisture method") is used that keeps track of dynamic changes in soil moisture and simultaneously calculates irrigation demand, GW recharge, evapotranspiration, interflow, and surface runoff, 3) multi-objective optimization is used to calibrate WEAP-MODFLOW model parameters using GW level and river discharge data, and 4) the calibrated model is applied to generate new quantitative insights of historical drought impacts in the Miyandoab plain. The paper is organized as follows. Section 2 describes the SW-GW model for the Miyandoab plain, including details of the SW, GW, and soil moisture parts of the model. Section 3 introduces the process of WEAP-MODFLOW calibration and describes the calibration parameters and calibration algorithm. Results and conclusions are presented in Section 4 and 5, respectively.

2. SW-GW model for the Miyandoab plain

2.1. Overview: GW and SW resources, hydrology and hydrogeology

Fig. 1 shows location of the Miyandoab Plain between 36° 50′ to 37° 15′ N and 45° 50′ to 46° 15′ E , with a total area of about 1524 km^2. The climate is semi-arid-cold with an average annual precipitation and temperature of ~290mm and ~14°C, respectively. Most of the precipitation falls from mid-autumn to mid-spring. Table S1 shows the monthly distribution of climate data in the plain. Spatial variations in rainfall are small due to the low elevation (~30m) of the plain.

SW supply originates from two important rivers: Zarrineh Rood and Simineh Rood. These rivers flow into Urmia Lake after crossing the Miyandoab Plain. Zarrineh Rood and Simineh Rood provide more than 40% and 10% of the total annual inflow into Urmia Lake, respectively (Ghaheri et al., 1999). Zarineh Rood is the largest river in Urmia basin and the average annual discharge of this river at the entrance of Miyandoab Plain is about 2000 MCM (Million Cubic Meters) per year (Fig. 1). Annual average discharge of the Simineh Rood River at the entrance of the Plain is about 340 MCM per year (Fig. 1). The other rivers running along the Miyandoab Plain are Lilan-Chai, Quri-Chai, and Mordaq-Chai, with a total discharge at the entrance of the Plain of about 84 MCM, 99 MCM, and

109 MCM per year, respectively. Bukan Dam is the only storage dam on the Zarineh Rood River with total and active storage capacities of 808 MCM and 654 MCM, respectively. The reservoir is used for flood control and water allocation to urban and agricultural water users in the Miyandoab Plain. The Norozloo diversion dam is located downstream of Bukan Dam. This dam is used to divert water into the primary irrigation canal of the Miyandoab irrigation and drainage network.

Total irrigated area is approximately 100,000 hectares, with about 58% and 42% allocated to (annual) crops and orchards, respectively. Crops include wheat, maize, alfalfa, sugar beet, and tomato, and orchards include apples, grapes, stone-fruits, almonds and conifer trees. The irrigated area is divided into internal agricultural zones (Z1, Z2, Z3, Z4, Z5, Z6, Z7, Z8, Z9-1, Z9-2, Z9-3, Z9-4, Z9-5, 2) and external agricultural zones (ZN, G, M1, M2, L1, L2, S, ZP), as shown in Fig. 1. The land slope of the internal zones is very low (less than 1.1 %). In addition, irrigation and drainage networks and pumping wells have been developed in the internal zones. These factors led to cultivation of the majority of land in the internal zones , except for zones Z9-1 to Z9-5, which are close to the salty margin of Lake Urmia. On the contrary, external zones consist of foothills and mountains without extensive aquifers, and, as such, cultivation is limited around rivers, with irrigation via traditional canals from rivers and pumping wells. Table S2 and Table S3 show the area of crops and orchards in each zone of the Miyandoab plain. Moreover, Table S4 shows planting and harvesting dates, growing season length, crop coefficients (k_c), and maximum rooting depths for crops and orchards. Irrigation uses a combination of SW and GW resources.
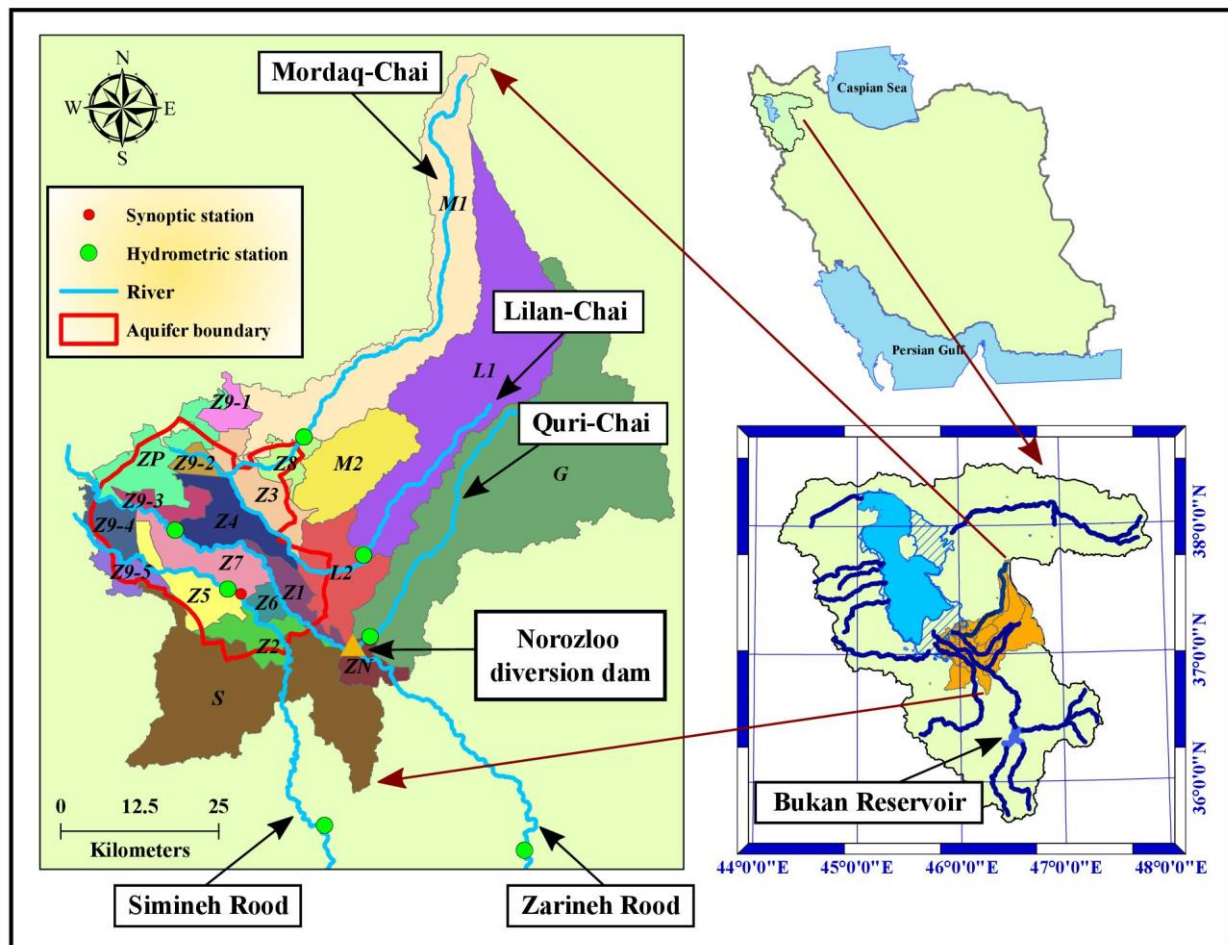

Fig. 1: Location of Urmia Lake basin and Miyandoab Plain, including numbered agricultural zones

4

Extent of the Miyandoab aquifer more or less coincides with the internal zones (Fig. 1). The Miyandoab aquifer consists of alluvial layers that form an alluvial fan, and marine and fluvial terraces. Well borehole data indicate that alluvial deposits are composed of gravel, sand, silt, and clay above the limestone bedrock of the aquifer. The Miyandoab aquifer is unconfined and the thickness of the alluvial layers approximately ranges from 40 m to more than 150 m. Well tests indicate that aquifer transmissivity ranges from 100 to 3000 m^2 per day and specific yield ranges from 0.12% to 8.7%. Extent of the aquifer in Fig. 2 is adopted from a previously developed GW model for the Miyandoab aquifer (Hamzehkhani et al., 2015). In that study, the lateral model boundaries were identified based on available lithological and geological maps, the location of operation wells, and observed groundwater levels. Specifically, in Fig. 2, the inflow and outflow lateral boundaries are parallel with isopotential lines, whereas the no flow boundaries are perpendicular to isopotential lines. There is significant GW inflow from the south and east boundaries of the aquifer which are located in the foothills of Sahand Mountain and the northern part of the Zagros Mountain, respectively. Moreover, there is significant GW outflow through the western and northern aquifer boundaries. Aquifer inflows include recharge due to irrigation, precipitation, infiltration from rivers, and inflows through the lateral boundaries. Aquifer outflows consist of GW withdrawal from almost 10,000 pumping wells, as well as drainage to the drainage network, the rivers, and through the lateral aquifer boundaries. Note that there is no aquifer in the external zones, and wells are limited to locations along the rivers. The following sections describe the concepts and methods used to simulate flow in the SW-GW system of the Miyandoab plain.
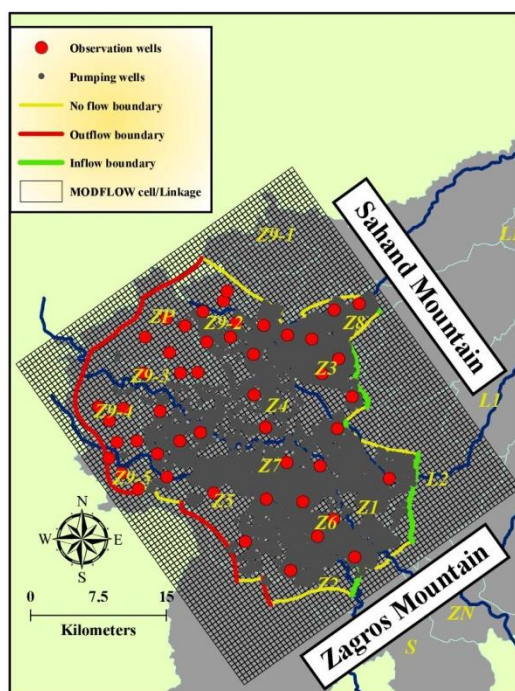

Fig. 2: GW flow grid for the Miyandoab aquifer, including lateral boundary conditions, and locations of pumping and observations wells
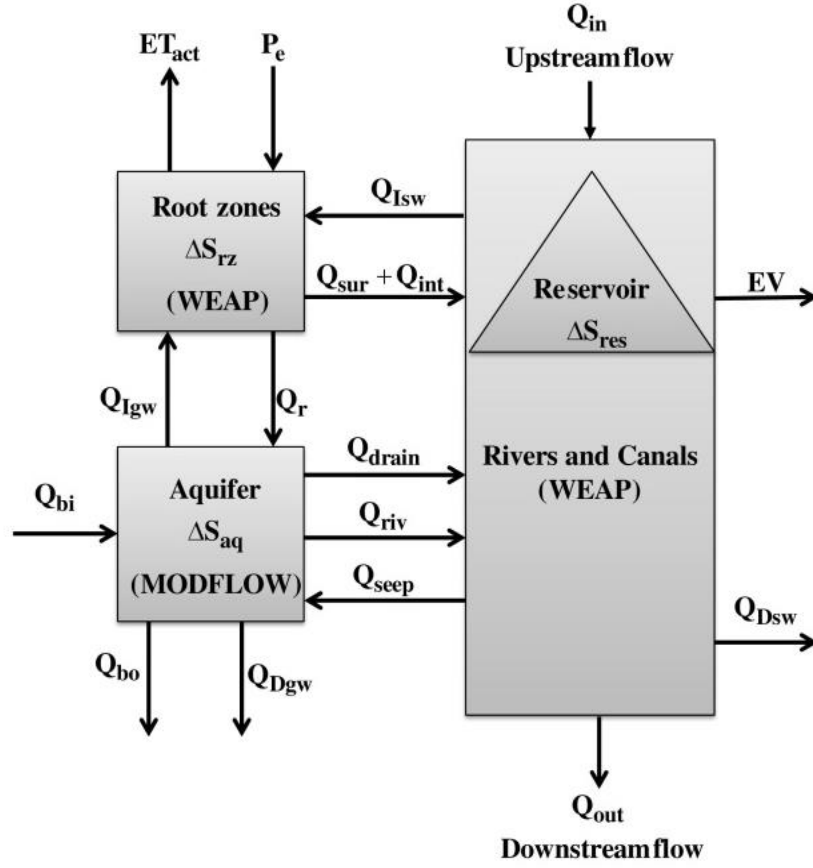
Fig. 3: Schematic diagram of the coupled SW-GW flow model. Variables are defined in Tables 1-4. Each model component is spatially discretized into interacting control volumes for which monthly water balances are formulated.

2.2. Mathematical description of the coupled SW-GW flow model

A schematic diagram of the coupled SW-GW flow model is presented in Fig. 3. The model includes the following interacting physical components: the root zone of agricultural crops, the underlying aquifer, surface reservoirs, rivers, and irrigation and drainage canals. Each of these components is spatially discretized into interacting control volumes for which monthly water balances are formulated. In the following paragraphs, each component is discussed in more detail.

Root-zone

The root-zone water balance equations and variables are summarized in Table 1. The root-zone water balance equations are applied monthly to each crop in each agricultural zone (Fig. 1). Each water balance computes changes in root-zone water storage as a function of inflows (irrigation with SW Q_{Isw} and GW Q_{Igw}, and effective precipitation P_e) and outflows (actual evapotranspiration ET_{ac}, surface runoff Q_{sur}, subsurface runoff (interflow) Q_{int}, and GW recharge Q_r). As shown in Table 1, these outflows are computed using empirical functions of relative soil water content z (varying between 0 and 1, corresponding to, respectively, dry and saturated soil), which are based on the "soil moisture method" implemented in WEAP (Sieber and Purkey, 2015; Yates et al., 2005). These empirical equations contain three calibration parameters: (i) Runoff Resistance Factor (*RRF*), which controls surface runoff (large values yield less runoff) and depends on land cover, (ii) Preferred Flow Direction (*f*), which controls partitioning of total subsurface outflows into interflow (horizontal) and GW recharge (vertical) and depends on land cover, soil, and topography, and (iii) root zone conductivity (*K*). Following the expression for groundwater recharge in Table 1, root zone conductivity parameter *K* is closely related to the maximum

6

groundwater recharge rate, which occurs when the soil is completely saturated ($z=1$). For example, in flat terrain, when $f\sim 0$, the maximum groundwater recharge rate is equal to K. The value for K is not necessarily equal to the saturated hydraulic conductivity of the soil (Galaitsi, 2018). An appropriate value for K is obtained here via calibration. Potential evapotranspiration in Table 1 is calculated using the standard Penman-Monteith method, while irrigation demand, i.e. the sum of SW and GW extractions ($Q_{Isw}+Q_{Igw}$), is computed as follows: irrigation starts when relative soil water content falls below a specified intervention value, z_{int}, and proceeds until a specified target value, z_{tar}, is reached (Sieber and Purkey, 2015). Climate, crop, and soil input data for these calculations are included in the supplement (Table S1-S4, S7).

Table 1: Root-zone water balance variables and equations, applied monthly to each crop in each agricultural zone (Fig.1).

Variable	Unit	Equation or data source
Storage change	L^3/T	$\dfrac{\Delta S_{rz}}{\Delta t}=nZ_r A\dfrac{\Delta z}{\Delta t}=Q_{Isw}+Q_{Igw}+P_e A-ET_{act}A-Q_{sur}-Q_{int}-Q_r$
Relative soil water content	-	$z_{t+1}=z_t+\Delta z$
Actual evapotranspiration	L/T	$ET_{ac}=(PET)k_c(\dfrac{5z-2z^2}{3})$
Irrigation Demand	L^3/T	$Q_{Isw}+Q_{Igw}=nZ_r A(z_{tar}-z_{int})$
Surface runoff	L^3/T	$Q_{sur}=(Q_{Isw}+Q_{Igw}+P_e A)z^{RRF}$
Interflow	L^3/T	$Q_{int}=fKz^2 A$
GW recharge	L^3/T	$Q_r=(1-f)Kz^2 A$
Porosity	-	n: Table S7
Rooting depth	L	Z_r: Table S4
Irrigated area for each crop in each zone	L^2	A: Table S2 and S3
Effective precipitation	L/T	P_e: based on separating total precipitation into rainfall and snowmelt using the method of (Yates et al., 2005) with input meteorological data from Miyandoab weather station (Iran Meteorological Organization, https://www.irimo.ir)
Potential evapotranspiration	L/T	PET: Penman-Monteith method using input meteorological data from Miyandoab weather station (Iran Meteorological Organization, https://www.irimo.ir)
Crop coefficient	-	k_c: Table S4
Target relative soil water content	-	$z_{tar}=1.0$ (for basin irrigation)
Intervention relative soil water content	-	$z_{int}=0.4$ (for basin irrigation). This value represents a soil saturation value in between field capacity and wilting point.
Runoff resistance factor	-	RRF: calibration parameter
Preferred flow direction	-	f: calibration parameter
Root zone conductivity	L/T	K: calibration parameter

Aquifer

The aquifer water balance equations and variables are summarized in Table 2. The aquifer water balance equations are applied monthly to each 500m-by-500m cell of a two-dimensional grid (Fig. 2) that horizontally covers the Miyandoab aquifer (approximately 920 km^2) and vertically extends from the unconfined water table to the underlying bedrock. The grid consists of 75 columns and 87 rows, resulting in a total of 6525 cells, and 3674 cells that fall within the aquifer boundary and for which a monthly water balance is included. Each water balance computes grid-cell changes in GW storage (and head) as a function of its inflows (GW recharge Q_r, seepage from

rivers Q_{seep}, lateral GW inflows Q_{bi}) and outflows (GW extraction for irrigation Q_{Igw} and drinking water Q_{Dgw}, GW discharge to rivers Q_{riv} and drains Q_{drain}, and lateral GW outflows Q_{bo}). GW recharge is an input from the root-zone water balance (Table 1), while GW extraction for irrigation Q_{Igw} and drinking water Q_{Dgw} are obtained using a water allocation procedure described in section 2.3. That procedure also ensures that GW extraction is not greater than available GW pumping capacity in each agricultural zone. The remaining flows are computed using Darcy-type equations of the form $C(h_1-h_2)$, where C is a hydraulic conductance, and h_1 and h_2 are two water levels: one representing hydraulic head (GW level) in the current cell, and the other either river water level (for river-aquifer interactions), drainage level (for GW flow to drains), or GW level of a neighboring cell or location (for lateral GW flows). The exact form of this equation for each flow is detailed in Table 2, along with the used data sources. Note that rivers can either feed (Q_{seep}) or drain (Q_{riv}) GW, depending on the relative position of GW and river water levels. In contrast, interaction between GW and drains (Q_{drain}) only happens in one direction: when GW level is below the drain elevation, no water exchange occurs between the two. Fig. 2 shows the external aquifer boundaries where inflow, outflow, or no flow occurs. Lateral GW flows across internal boundaries (between cells) and storage change depend on two spatially variable calibration parameters: aquifer hydraulic conductivity K_h and specific yield S_y.

Table 2: Aquifer water balance variables and equations, applied monthly to each GW flow grid cell (Fig. 2).

Variable	Unit	Equation or data source
Storage change	L^3/T	$\frac{\Delta S_{aq}}{\Delta t} = A\,S_y\,\Delta h = Q_r + Q_{seep} + Q_{bi} - Q_{Igw} - Q_{Dgw} - Q_{riv} - Q_{drain} - Q_{bo}$
Hydraulic head	L	$h_{t+1} = h_t + \dfrac{\Delta h}{\Delta t}$
Lateral GW flows	L^3/T	$Q_{bi} = \sum_b C_b (h_b - h)^*$ for $h < h_b$ $Q_{bo} = \sum_b C_b (h - h_b)$ for $h > h_b$
Recharge	L^3/T	Q_r: see Table 1
GW extraction for irrigation	L^3/T	Q_{Igw} : water allocation procedure described in section 2.3
GW extraction for drinking	L^3/T	Q_{Dgw}: water allocation procedure described in section 2.3
Discharge to river	L^3/T	$Q_{riv} = C_R (h - h_{bot} - d)$ for $h < h_{bot}$
Seepage from river	L^3/T	$Q_{seep} = C_R (h_{bot} + d - h)$ for $h \geq h_{bot}$
Discharge to drain	L^3/T	$Q_{drain} = C_d (h - h_d)$
River water depth	L	d: Table 4
Specific yield	-	S_y: calibration parameter
Hydraulic conductivity	L/T	K_h: calibration parameter
Grid cell area	L^2	$A = (500\ \text{m})^2$
River bed conductance	L^2/T	C_R: (Ministry of Energy of Iran, 2014)
River bed elevation	L	h_{bot}: (Ministry of Energy of Iran, 2014)
Drain conductance	L^2/T	C_d: (Ministry of Energy of Iran, 2014)
Drain elevation	L	h_d: (Ministry of Energy of Iran, 2014)
Boundary conductance	L^2/T	C_b: input data (Ministry of Energy of Iran, 2014) for external boundaries $C_b = \overline{(K_h)h}$ for internal boundaries**
Boundary head	L	h_b: input data (observed GW heads) for external boundaries h_b: GW head in neighboring grid cell for internal boundaries

* Index b sums over the 4 boundaries of a square grid cell.

** $\overline{(K_h)h}$ denotes the harmonic average of transmissivity $(K_h)h$ between two neighboring grid cells.

Reservoirs

The reservoir water balance equations and variables are summarized in Table 3. The reservoir water balance equations are applied monthly to Bukan storage reservoir. Water balance computes changes in the reservoir storage as a function of inflows (precipitation $A_{res}P$ and upstream inflow Q_{in}) and outflows (evaporation $A_{res}E$ and release R for irrigation and drinking demand). Reservoir release is obtained as the sum of drinking water demands and irrigation demand computed in each agricultural zone (see Table 1), subject to the constraint that releases from dead storage (S_{dead}) are not possible. Note that releases may be larger than total water demand when the reservoir is completely full and overtopping occurs. Reservoir surface area (A_{res}) is computed using a volume-area-elevation function f that depends on reservoir storage (S_{res}) and uses linear interpolation between observed (A_{res}, S_{res}) pairs.

Table 3: Reservoir water balance variables and equations, applied monthly to Bukan reservoir (Fig. 1).

Variable	Unit	Equation or data source
Storage change	L^3/T	$\frac{\Delta S_{res}}{\Delta t} = Q_{in} - R + A_{res}P - A_{res}E$
Storage	L^3/T	$S_{t+1} = S_t + \Delta S$
Upstream inflow	L^3/T	Q_{in}: input data (Ministry of Energy of Iran, 2016)
Downstream release	L^3/T	$R = \min(S - S_{dead}, \sum Q_{Dsw} + \sum Q_{Isw})$
Precipitation rate	L/T	P: input data (Ministry of Energy of Iran, 2016)
Evaporation rate	L/T	E: input data (Ministry of Energy of Iran, 2016)
Reservoir surface area	L^2	$A_{res} = f(S_{res})$

Rivers and canals

The river/canal water balance equations and variables are summarized in Table 4. The river/canal water balance equations are applied monthly to each river and canal reach. In contrast to the other components, monthly storage changes in river and canal reaches are neglected. As such, each water balance computes outflow Q_{out} from the reach as a function of inflows (upstream inflow Q_{in} into the reach, irrigation return flows (surface runoff Q_{sur}, interflow Q_{int}), GW discharge to rivers Q_{riv} and drains Q_{drain}) and outflows (SW extraction for irrigation Q_{Isw} and drinking water Q_{Dsw}, and seepage into the aquifer Q_{seep}). Note that direct evaporation is neglected in the water balance of both rivers and canals. SW extraction from each river and canal reach to meet water demand is computed, together with GW extractions, using a water allocation procedure described in section 2.3. The SW-GW interaction terms depend on water depth in each reach (see formulas in Table 2). Water depth d is computed using a flow-depth function f that depends on river discharge Q_{out} and uses linear interpolation between observed (d, Q_{out}) pairs. As indicated in Table 4, canal reaches do not interact with the aquifer as irrigation canals are lined.

Table 4: River/canal water balance variables and equations, applied monthly to each river and canal reach.

Variable	Unit	Equation or data source
Downstream outflow	L^3/T	$Q_{out} = Q_{in} - Q_{Isw} - Q_{Dsw} - Q_{seep} + Q_{riv} + Q_{sur} + Q_{int} + Q_{drain}$
Upstream inflow	L^3/T	Q_{in}: input data (Ministry of Energy of Iran, 2016), outflow from upstream reach, or release from upstream reservoir
SW extraction for irrigation	L^3/T	Q_{Isw}: water allocation procedure described in section 2.3
SW extraction for drinking water	L^3/T	Q_{Dsw}: (Ministry of Energy of Iran, 2016)
Irrigation return flows	L^3/T	Q_{sur}, Q_{int}: Table 1
GW interaction terms	L^3/T	Q_{seep}, Q_{riv}, Q_{drain}: for rivers see Table 2; for canals these terms are zero
Water depth	L	$d = f(Q_{out})$

Table 5: Implementation of model components and flows in WEAP-MODFLOW

Model component or flow	Implemented with	Implemented as	For each (number)
Root zone	WEAP	Catchment node	Agricultural zone (21)
Reservoir	WEAP	Reservoir node	Reservoir (1)
Rivers and their tributaries	WEAP	River element	River reach (26)
Primary canals	WEAP	Diversion	Canal reach (5)
Urban (Drinking) demand	WEAP	Demand site node	City (3)
Surface runoff and interflow	WEAP	Runoff and infiltration link	Agricultural zone (21)
SW extraction for irrigation	WEAP	Transmission link	Agricultural zone (21)
SW extraction for drinking	WEAP	Transmission link	City (3)
Aquifer**	WEAP / MODFLOW	GW node / Block-centered flow packages	Agricultural zone (13) / Grid cell
Local Aquifer**	WEAP	GW node	Agricultural zone (8)
GW extraction for irrigation	WEAP / MODFLOW	Transmission link / Well package	Agricultural zone (21) / Pumping well
GW extraction for drinking	WEAP / MODFLOW	Transmission link / Well package	City (1) / Pumping well
GW recharge	WEAP / MODFLOW	Runoff and infiltration link / Recharge package	Agricultural zone (21) / Grid cell
River-aquifer interaction	MODFLOW	River package	River reach (4)*
GW drainage	MODFLOW	Drain package	Grid cell
Other demand (Saeen Ghaleh irrigated area and Evaporation of Norouzlo dam)	WEAP	Demand site node	Demand site (2)
SW extraction for Other demand	WEAP	Transmission link	Demand site (2)

* 4 river reaches are the sections of Zarineh Rood, Simineh Rood, Lilan-chay, and Mordaq-Chai on top of the aquifer (Fig. 1)

** The boundary of the Miyandoab aquifer more or less coincides with extent of the internal agricultural zones, and we use symbol "Aquifer" for this. In all other zones, pumping wells are typically drilled around rivers and these wells are not connected to the Miyandoab aquifer and we use symbol "Local Aquifer" for this.

2.3. Implementation of the coupled SW-GW flow model in WEAP-MODFLOW

The coupled SW-GW model described in the previous section was implemented using the WEAP modeling tool (Sieber and Purkey, 2015; Yates et al., 2005) with a dynamic coupling to MODFLOW (Harbaugh, 2005). Table 5 gives an overview of how each component of the coupled SW-GW flow model is represented in WEAP-MODFLOW.

WEAP

As listed in Table 5, the model components are implemented using various spatial elements available in WEAP, called "nodes" and "links". Fig. 4 shows the spatial layout of these elements in WEAP. For example, the root zone component of the model was implemented as a collection of "Catchment nodes", one for each agricultural zone, that use the "soil moisture method" in WEAP for computing the various water balance components (as in Table 1). Each catchment node was further divided into two sub-catchments, one for crops and the other for orchards, and each sub-catchment was subdivided into individual crop types (Table S2 and S3). The reservoir of Bukan Dam was implemented as a "Reservoir node" with required inputs as in Table 3 (storage capacity, volume-elevation curve, monthly evaporation rate, and operation data) entered into WEAP. Evaporation volume from the reservoir of the Norouzlo dam was implemented in WEAP as a "Demand site". All rivers and their 21 tributaries were implemented as "River" elements in WEAP, with upstream inflows for Zarineh Rood and Simineh Rood rivers provided from

10

observation data of hydrometric stations that exist upstream of these rivers. The upstream flows of other rivers were characterized according to the official report for Miyandoab plain (Ministry of Energy of Iran, 2016). SW extractions from the Zarineh Rood river are routed to the primary irrigation canal in the Miyandoab irrigation and drainage network. This primary irrigation canal is implemented in WEAP as "Diversion" with a maximum diversion capacity based on its dimensions. WEAP "Demand sites" are used to account for drinking (urban) water demands in Tabriz, Bukan, and Miyandoab counties, and for irrigation demand of the "Saeen Ghaleh" area located between Bukan Dam and Miyandoab plain. Monthly water demand data for these were taken from official reports (Ministry of Energy of Iran, 2016). Each agricultural zone is also assigned a "GW node" in WEAP to represent GW storage and flows for that zone, together with maximum pumping capacities ("Maximum Withdrawal" in WEAP) for each zone according to total capacity of pumping wells in each zone. Finally, all nodes are connected using "links" in WEAP, which define the flow of water between spatial elements (model components). Two types of links are used: "Transmission links" and "Runoff and infiltration links". Runoff and infiltration links are used to (i) connect the catchment node in each agricultural zone (i.e. the root zone component for that zone) with the river element (river reach) that receives its irrigation return flows (surface runoff and interflow), and (ii) connect catchment and GW nodes in each zone to allow GW recharge from the root zone to the aquifer component of the model. Transmission links are used to connect catchment nodes to river elements and GW nodes to represent irrigation water extraction from, respectively, SW and GW components to the root-zone component of each zone. In other words, transmission links are used to implement the secondary irrigation canals in the irrigation and drainage network, as well as the traditional canals.

Finally, a water allocation procedure (Yates et al., 2005) available in WEAP is used to determine SW and GW extractions given drinking water demand (from data) and irrigation water demands computed in each root-zone water balance (Table 1). The procedure is formulated and solved as a linear program: it optimizes satisfaction of irrigation and drinking demand, subject to water supply preferences, water demand priorities, water balances, non-negativity constraints, and diversion and pumping capacity constraints. In this study, two types of water demand (irrigation and drinking) need to be met by two water supply sources (SW and GW). Drinking and agricultural demand priorities are set to 1 and 2, respectively, while SW and GW supplies are assigned preference ranks of 1 and 2, respectively, to indicate that GW extraction only occurs if water demands cannot be met by SW alone. The final outcome of the allocation procedure, which is repeated each month, are values for SW and GW extraction for each river reach resp. agricultural zone. These values serve as inputs for the aquifer water balances (Table 2) and the river water balances (Table 4).
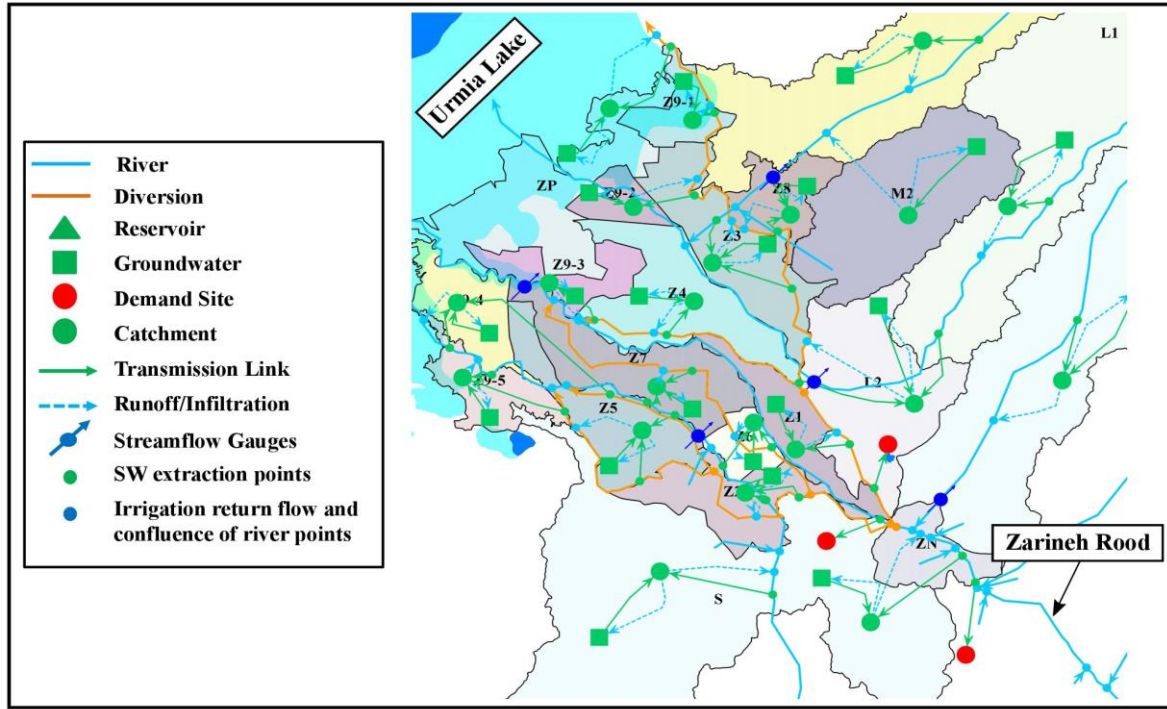
Fig. 4: Spatial elements in WEAP that represent interacting model components. Note that Bukan Reservoir and a demand site are located further upstream on the Zarineh Rood river.

WEAP-MODFLOW coupling

Implementation of the GW flow model in MODFLOW involves preparation of various input files, one for each MODFLOW "package". The GW flow grid (Fig. 2) is implemented via the Basic and Discretization packages, spatially variable aquifer parameters and properties are specified via the Block-Centered flow package, and interactions with the other model components are implemented using Recharge, Well, River and Drain packages (Table 5). Input data on topography, bedrock elevation, starting GW head, evapotranspiration, pumping wells, observation wells, rivers, and drains were obtained from the official report for the Miyandoab aquifer in 2010-2011 (Ministry of Energy of Iran, 2014). Lateral GW flow through the aquifer boundaries (Fig. 2) was specified using computed flows during the calibration period 2010-2011 (see section 3). The coupling of MODFLOW and WEAP is achieved via a GIS shape file that maps MODFLOW grid cells to WEAP spatial elements, i.e. catchment and GW nodes in each agricultural zone, and river elements. The shape file's attribute table has a record for each active MODFLOW grid cell that contains cell row, cell column, and identifiers for the relevant WEAP elements. As such, this linkage shape file allows dynamic data transfer between WEAP and MODFLOW. Specifically, the coupling involves the following steps: (1) GW recharge, pumping rates, and river water levels computed by WEAP are sent to MODFLOW as inputs, (2) MODFLOW input files are updated and the model is run for a single stress period (one month), and (3) MODFLOW simulated output for GW heads, lateral GW flows, and river-aquifer interactions are sent back to WEAP as input. This feedback between WEAP and MODFLOW is done for each month and this process continues until the end of the simulation period. The WEAP model calculates the total value of GW recharge of each agricultural zone and assigns this value uniformly to all MODFLOW grid cells within an agricultural zone. As mention before, the boundary of the Miyandoab aquifer approximately coincides with extent of the internal agricultural zones, excluding zone Z91 and including external agricultural zone ZP. Therefore, the GW nodes of these zones in WEAP model are all linked to MODFLOW. In all other zones, pumping wells are typically drilled around rivers and these wells are not connected to the Miyandoab aquifer and thus not linked to

12

MODFLOW. For more details about coupling WEAP and MODFLOW, please see these references: (Droubi et al., 2008a; Wolfer, 2009a, 2009b).

3. WEAP-MODFLOW calibration

3.1. Calibration parameters and data

Calibration parameters (Table 1 and 2) include root zone conductivity (K), runoff resistance factor (RRF), preferred flow direction (f), aquifer hydraulic conductivity K_h, and aquifer specific yield S_y. According to the location of hydrometric stations with river discharge data, the Miyandoab plain was divided into four calibration regions (Fig. 5). Calibration was split up into three sequential steps.
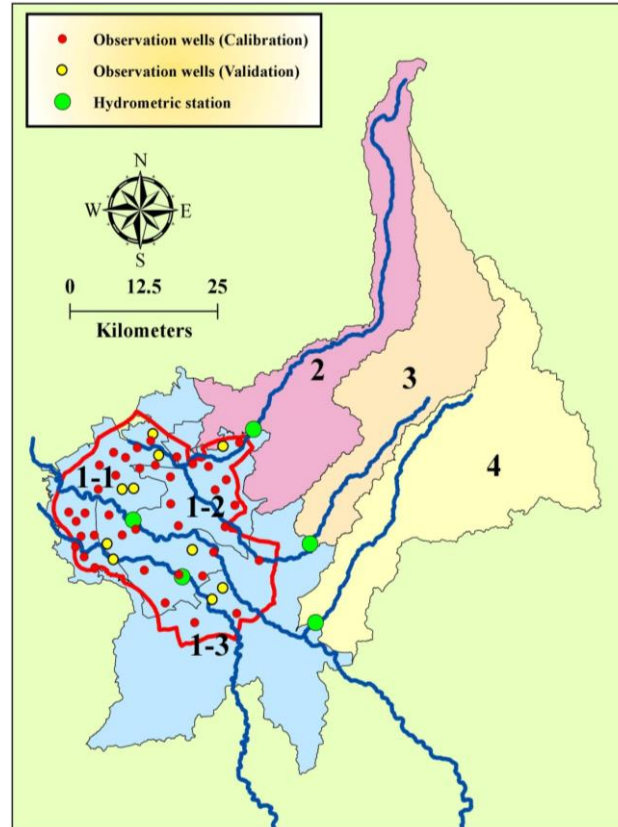

Fig. 5: Four calibration regions in Miyandoab plain

Calibration step 1

Regions 2, 3 and 4 in Fig. 5 are not linked to the MODFLOW model, and each of these regions has a hydrometric station at the outlet. In these three regions, PEST (Yates et al., 2005) was used to calibrate the three root zone parameters (*K, RRF, f*) using streamflow data of hydrometric stations from 2001 to 2013. Table S5 presents prior ranges for calibration parameters in calibration regions 2, 3, and 4.

Calibration step 2

The next step was to calibrate spatially variable aquifer hydraulic conductivity and specific yield values in the MODFLOW model. This was done separately (decoupled) from WEAP, and did not use GW recharge and pumping computed by WEAP. Instead, pumping was specified based on data, GW recharge from precipitation was estimated using the Hydrologic Assessment of Landfill Performance (HELP) model, and GW recharge from irrigation was estimated based on calculated net irrigation requirements using the Crop-Wat program (Clarke et al., 1998) combined with FAO coefficients of irrigation efficiency and GW recharge due to irrigation (FAO, 1980). A

more detailed description of the HELP model and the FAO coefficients is given in the supplement (See Table S6-S11). Initial conditions were based on interpolated observed GW level at the beginning of the simulation. The MODFLOW model was calibrated using annual (steady-state) and monthly (transient) time steps during the period 2010-2011, which is the only year that GW extraction data are available. In steady state, the inflow and outflow boundaries were considered as Specified Head Boundary and the other parts were considered as No Flow. The Specified Head Boundary in steady state was then translated into a General Head Boundary for the transient flow simulation. We used the yearly average of observed GW level for specified head along boundaries in steady state and the monthly observed GW level for General head along boundaries in transient mode. Note that this is different from the coupled WEAP-MODFLOW model, which uses specified flux conditions for the boundary flows: these specified flow values were based on simulated values using the calibrated MODFLOW model for 2010-2011. There are measured hydraulic conductivity and specific yield at some locations in the Miyandoab aquifer. The measured hydraulic conductivity changes between 2.08 m/day to 39.97 m/day, and the measured specific yield changes between 0.0012 to 0.087 (Ministry of Energy of Iran, 2014). Two calibration methods were used to estimate the calibration parameters, namely pilot points and zonation patterns for calibrating hydraulic conductivity and specific yield, respectively. Fig. S.1 shows the location of pilot points and parameter zones. PEST (Doherty, 2003) was used for automatic calibration of the parameters.

Calibration step 3

The final step, which will also be focus of the results section, is calibration of region 1. For this step the coupled WEAP-MODFLOW model was used, with aquifer parameters (K_h and S_y) fixed as obtained in the previous step and root zone parameters (K, RFF, f) as calibration parameters. Irrigation in region 1 affects both runoff of two hydrometric stations located on the Zarrineh Rood and Simineh Rood rivers, and GW heads of observation wells in the Miyandoab aquifer. Therefore, there are two types of data for the calibration of region 1, and multi-objective optimization was used. In this regard, the following assumptions were made for region 1:

- The land surface slope is very low and this part of the plain is approximately flat. Therefore, the interflow in this region is close to zero and the value of the preferred flow direction parameter *f* is assumed to be zero.
- The Runoff Resistance Factor parameter was considered separately for crops and orchards.
- For calibration of root zone conductivity, region 1 was divided into three sub-regions based on soil type: the lower region (region 1-1), the middle region (region 1-2), and the upper region (region 1-3).

As such, 5 parameters were subject to calibration in region 1, as listed in Table 6. Initial ranges for the parameters were selected based on Sieber and Purkey, (2015) and a literature review (e.g. Ingol-Blanco and McKinney, 2012; Yates et al., 2005). Root Mean Square Error (*RMSE*) is used to evaluate model performance:

$$RMSE_i = \sqrt{\frac{\sum_{t=1}^{T_i}(Obs_i(t) - Sim_i(t))^2}{T_i}} \qquad (1)$$

where *i* indicates the type of observation data (streamflow "*Q*" and GW head "*aq*"), $RMSE_i$ is the root mean square error for data type *i*, T_i is the number of measurements of data type *i*, $Obs_i(t)$ is the observation of data type *i* at time *t*, and $Sim_i(t)$ is the corresponding simulated value. Ideally, an optimal parameter set is identified that minimizes the two objective functions together. However, this is not typically possible due to errors in the hydrological model.

14

Therefore, the trade-offs between matching the different objectives were investigated by performing a multi-objective calibration and evaluating the tradeoff relations in the Pareto front of $RMSE_Q$ vs $RMSE_{aq}$.

To ensure a good spatial coverage in region 1, 39 observation wells shown in Fig. 5 were selected for calibration. Monthly observed GW levels from these wells for the period 2008-2013 were used for calibration, as well as monthly observed river discharge (sums of daily observed values) for hydrometric stations in Fig. 5 for the period 2001-2013. Data used for independent validation of the model include: (1) monthly observed GW levels for 10 observation wells not used in the calibration during the period 2001-2013, (2) monthly observed river discharge for all hydrometric stations for the period 1991-2001, and (3) observed storage volume in Bukan Dam reservoir for the period 1991-2013. Table 7 summarizes the calibration and validation process.

Table 6: Calibration parameters in calibration region 1

Parameter	Description	Unit	Min	Max
K1	Root Zone Conductivity for region 1-1	mm/month	10	250
K2	Root Zone Conductivity for region 1-2	mm/month	10	250
K3	Root Zone Conductivity for region 1-3	mm/month	10	250
RRF1	Runoff Resistance Factor for crops in region 1	No unit	0	10
RRF2	Runoff Resistance Factor for orchards in region 1	No unit	0	10

Table 7: Summary of the calibration and validation process in each calibration step

Calibration Step	Parameters	Description	Model	Data	Calibration Period	Validation Period
1	RRF, K, f	Calibration parameters for region 2, 3, and 4	WEAP	Stream flow	2001-2013	1991-2001
2	K_h, S_y	Calibration parameters for Miyandoab aquifer	MODFLOW	GW level	2010-2011	2001-2013
3	RRF, K	Calibration parameters for region 1	Coupled WEAP-MODFLOW	Stream flow	2001-2013	1991-2001
				GW level	2008-2013	2001-2013

3.2. Multi-objective calibration algorithm

Multi-Objective Particle swarm optimization (MOPSO) was used for calibration. This is a method inspired by the flocking behavior of birds. It is a population-based algorithm that combines individual learning and social behavior. In this algorithm, an external repository is used to store non-dominated parameter sets or "solutions" (Coello et al., 2004). The algorithm starts by generating an initial population of particles x_i, where each particle holds a 5-dimensional parameter set, in this case the set {*K1, K2, K3, RRF1*, and *RRF2*}. All particles of this population are compared to each other in terms of $RMSE_{aq}$ and $RMSE_Q$, and the non-dominated particles are stored in the repository. The parameter set of each particle is subsequently updated, from iteration t to iteration $t+1$, using the following equations:

$$v_i(t+1) = w\,v_i(t) + r_1(P_i(t) - x_i(t)) + r_2(R_h(t) - x_i(t)) \qquad (2)$$
$$x_i(t+1) = x_i(t) + v_i(t) \qquad (3)$$

where, w is an inertia coefficient ($w = 0.4$), r_1 and r_2 are uniform random numbers between 0 and 1, P_i is the current best performing parameter set for particle i, R_h is a parameter set selected from the external repository in each iteration t, as discussed below, and $v_i(t)$ is current "velocity" of particle i (Coello et al., 2004). The first value of P_i is equal to the initial parameter set of particle i and then is updated in the following way: (1) if the current $P_i(t)$

dominates the new parameter set $x_i(t+1)$ then set $P_i(t+1)=P_i(t)$, (2) if the new parameter set $x_i(t+1)$ dominates $P_i(t)$ then set $P_i(t+1)=x_i(t+1)$, or (3) if no one dominates the other then one of them is randomly set equal to $P_i(t+1)$. In MOPSO, there are several equally good non-dominated parameter sets stored in the external repository. One of the parameter sets stored in the repository is chosen by the algorithm as R_h to update the velocity of each particle using Eq. 3. Non-dominated parameter sets located in regions more densely populated in the objective space have a lower probability to be selected. This selection leads to better distributions of parameter sets on the Pareto front. In every iteration t, the new parameter sets of all particles are compared with each other and the non-dominated ones are then compared with all parameter sets stored in the repository. The repository is then updated, adding new non-dominated parameter sets and eliminating old parameter sets that are now dominated. The size of the external repository is an important parameter of the algorithm. Once the repository is full, a new non-dominated parameter set must take the place of another non-dominated parameter set in the repository. The parameter set to be replaced is selected randomly using a similar procedure as described previously, such that parameter sets located in denser regions of the objective space have higher probabilities of being selected. As the last step in each iteration, a mutation operator is employed to enhance the global search capability of the algorithm. The operator randomly changes the parameter sets of a fraction of particles in the population. This fraction is exponentially reduced with the number of iteration at a rate defined by the user. The process continues until reaching the maximum number of iterations. More details about MOPSO are provided by Coello et al. (2004).

4. RESULTS AND DISCUSSION

The results section is organized as follows. First, results of the multi-objective calibration of the coupled WEAP-MODFLOW model are presented, including a discussion of the obtained parameter values and a validation using independent observations. Second, the calibrated (and validated) model is used to gain new quantitative insights into historical hydrological changes in the Miyandoab Plain. Specifically, we present computed water balances for each component (rivers, root zone, aquifer) and quantify historical drought impacts on the hydrology of the Miyandoab Plain.
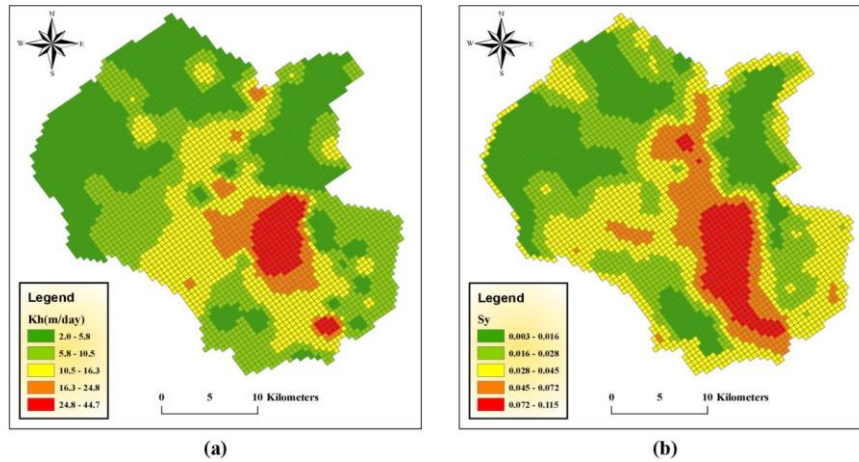
4.1. Calibration results of step 1 and step 2

Calibrated parameter values for calibration of regions 2, 3, 4 in step 1 are shown in Table 8. These parameters were calibrated by running PEST directly from within the WEAP software. The calibrated range of K is between 175 mm/month and 209 mm/month in all cases, and these values have a small range compared to the initial range in Table S5. The range of f is between 0.11 and 0.21 in all cases, and these values have a small range compared to the initial range in Table S5. The land slope of regions 2, 3, and 4 are 15%, 11.4%, and 9%, respectively. As expected, increasing land slope corresponds to a larger value for f (preferred flow direction) increase. The range of *RRF* crop and *RRF* orchards is between 1.35 and 2.2 in all cases, and these values have a small range compared to the initial range in Table S5. Values for *RRF* orchards tend to be a bit larger than *RRF* crop, suggesting that crops are more prone to runoff generation than orchards. *RMSE* values for simulated streamflow range from 0.5 to 1.2 m3/s (Table S12), and monthly dynamics in streamflow are well reproduced by the model, both in calibration (Fig. S2) and validation (Fig. S3).

Table 8: Calibrated parameter values for calibration regions 2, 3, and 4

Calibration region (Fig. 5)	Agricultural Zone (Fig. 1)	K(mm/month)	f	RRF Crop	RRF Orchards
2	M1 and M2	208.57	0.21	1.35	1.90
3	L1 and L2	164.97	0.16	1.44	1.83
4	G	175.36	0.11	1.57	2.19

Proceeding to results of calibration step 2, Fig. 6 shows maps of calibrated values of aquifer hydraulic conductivity and specific yield. The range of calibrated hydraulic conductivity is between 2 m/day to 44.7 m/day, and the range of calibrated specific yield is between 0.003 to 0.115. These values correspond with measured values cited earlier. The range and spatial distribution of calibrated hydraulic conductivity and specific yield values are also in good agreement with previous groundwater studies in the Miyandoab aquifer (Hamzehkhani et al., 2015; Ministry of Energy of Iran, 2014). Scatter plots between observed and simulated GW levels (Fig. S4) show good agreement: for the steady–state calibration, the Mean Error (*ME*), the Mean Absolute Error (*MAE*), and the Root Mean Square Error (*RMSE*) were 0.025, 0.528, and 0.641 meters, respectively; for the transient flow calibration, these respective values become 0.045, 0.797, and 1.022 meters. Moreover, the relative error ranges from 0 to 0.11% for steady state, and from 0 to 0.62% for transient flow. Finally, the computed groundwater balance agrees well with previous studies, providing further confidence in validity of the groundwater model (Table S13).

Fig. 6: Calibrated values for (a) hydraulic conductivity and (b) specific yield

4.2. Calibration results of step 3 (Multi-objective calibration)

Fig. 7 shows results of the multi-objective calibration with the MOPSO algorithm after 2500 model simulations. In this study, the used computer has a CPU speed of 3.7 GHz and 16 GB of memory installed (RAM), and for each coupled WEAP-MODFLOW model run for the period 2001-2013 takes 5 minutes on average. Based on the Pareto front, there is relatively little trade-off between minimizing the $RMSE_{aq}$ and $RMSE_Q$ objective functions, indicating that improvement in the fit of one objective function does not significantly affect the fit of the other objective function. This suggests that there are no large errors in the model that prevent a simultaneous fit to GW levels and river discharge. Fig. 8 shows scatter plots for the two objective functions ($RMSE_{aq}$ and $RMSE_Q$) against all five calibration parameters. These results show that $RMSE_Q$ is sensitive to the value of $K2$, i.e. root zone conductivity of region 1-2, and to a lesser extent also to the value of $K3$ (root zone conductivity of region 1-3). Furthermore, $RMSE_{aq}$ is most sensitive to the root zone conductivity of region 1-1 ($K1$), and the two objective functions agree on optimal ranges for the $RRF1$ and $RRF2$ parameters. Fig. 8 indicates that larger values for $K2$ and $K3$ lead to smaller

$RMSE_Q$, while smaller values for $K1$ lead to smaller $RMSE_{aq}$. These results reflect differences in land use and soil type between region 1-1 and regions 1-2 and 1-3. The latter are dominated by agricultural crops and loamy soils, whereas region 1-1 is located near Urmia lake and contains salt marshes and limited agricultural land. Therefore, the volume of surface runoff generated from irrigation is larger in regions 1-2 and 1-3, resulting in greater sensitivity of simulated streamflow to parameter K. Conversely, the main source of GW recharge in region 1-1 is precipitation, making simulated GW recharge in this region sensitive to parameter K.
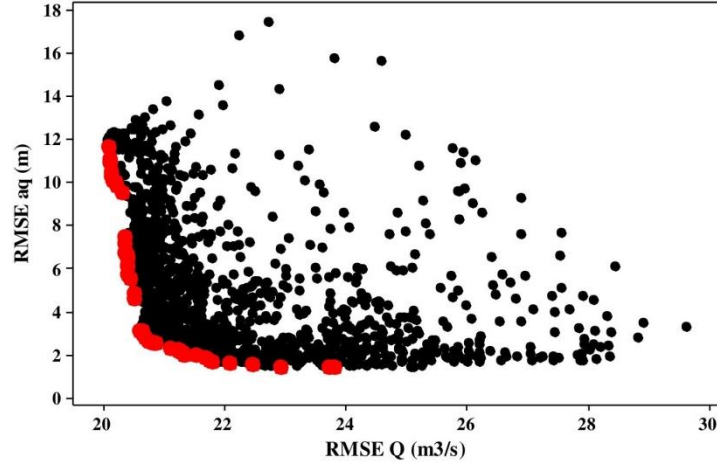
Fig. 7: Pareto plot for the multi-objective calibration after 2500 model simulations with the MOPSO algorithm. Each point shows one simulation of the WEAP-MODFLOW model and red points indicate the Pareto front, i.e. the set of non-dominated simulations.

Table 9 summarizes calibrated parameter values corresponding to minimal $RMSE_{aq}$, minimal $RMSE_Q$, and minimal Euclidean distance in $RMSE_{aq}$-$RMSE_Q$ space. The range in calibrated values of $RRF1$ and $RRF2$ is small compared to the initial ranges for these parameters (Table 6), suggesting that both these parameters are well identified and independent of the objective function used. On the contrary, calibrated values of $K1$, $K2$, and $K3$ differ significantly depending on the objective function used. The reason is that the two objective functions are sensitive to different calibration parameters. For example, the streamflow objective is very sensitive to $K2$ and $K3$, while the aquifer head objective is not. Table 9 further shows that the parameter values that minimize Euclidean distance are close to the values of the most sensitive calibration parameters obtained by minimizing the objective functions separately. For example, the value of $K1$ for the minimal Euclidean distance is 35.19, which is close to the value of $K1$ (23.641) that minimizes $RMSE_{aq}$. Similarly, values of $K2$ and $K3$ that minimize $RMSE_Q$ are close to the values of $K2$ and $K3$ that minimize Euclidean distance. Finally, we note that the smaller value of $K1$ compared to $K2$ and $K3$ makes sense: soils in region 1-1 are a mixture of clay, silt and salt whereas regions 1-2 and 1-3 consist of loam soils.

To gain further insights into parameter identifiability and information content of the data, Fig. 9 presents box plots of each calibration parameter for three cases: parameter sets on the Pareto front, parameter sets for which $RMSE_Q$<22.5 m³/s, and parameter sets for which $RMSE_{aq}$<8m. In all three cases, the median of $K1$ is less than 100 mm/month, with the interquartile range of $K1$ smallest for the case $RMSE_{aq}$<8m, confirming that GW level observations contain more information about parameter $K1$ than do river discharge observations. The medians of $K2$ and $K3$ are consistently greater than 200 mm/month. Parameter $K2$ has the smallest interquartile range for the case $RMSE_Q$<22.5 m³/s, suggesting that river discharge observations contain more information on this parameter than do GW level observations. For the remaining parameters ($K3$, $RRF1$, $RRF2$) we see that combination of the

two datasets (as in the Pareto case) yields the smallest interquartile range and thus the best identified parameter values, compared to only using one of the datasets. Fig. 9 further shows that the medians of *RRF1* (*RRF* crop) and *RRF2* (*RRF* orchards) are less than 1.8 and that their interquartile range lies between 1.3 and 2.2 in all cases. Values for *RRF2* tend to be a bit larger than *RRF1*, suggesting that crops are more prone to runoff generation than orchards. Overall, the combination of GW levels and river discharge data yields well identified parameters, which is further confirmed by the low parameter correlation coefficients reported in Table 10: the largest correlation is 0.26 between *K1* and *K3*.
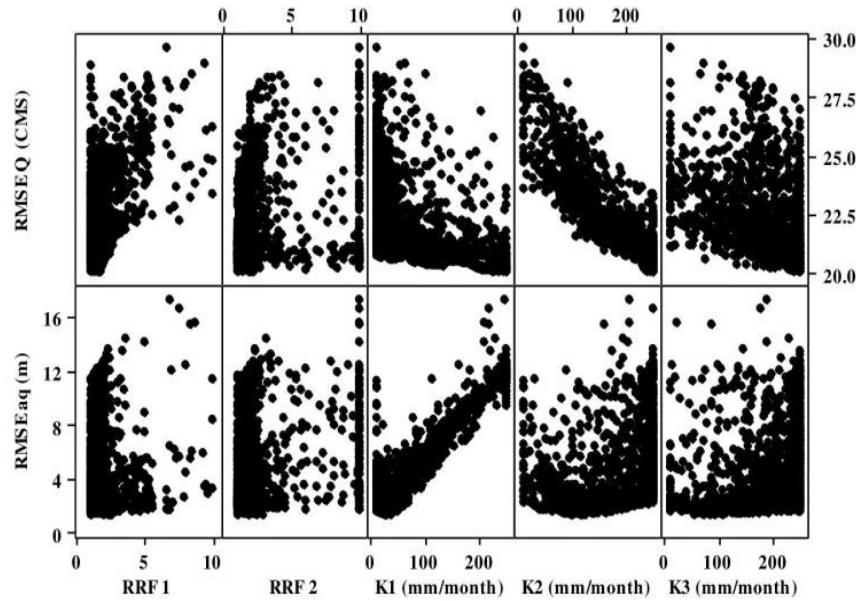

Fig. 8: Scatter plots for the two objective functions against all five calibration parameters

Table 9: Calibrated parameter values and corresponding *RMSE* values for calibration and validation periods

Process	Parameter	Minimal $RMSE_O$	Minimal $RMSE_{aq}$	Minimal Euclidean distance
Calibration	*RRF1* (-)	1.55	1.52	1.59
	RRF2 (-)	1.79	1.76	1.71
	K1 (mm/month)	243.66	23.64	35.19
	K2 (mm/month)	250.00	117.25	245.20
	K3 (mm/month)	244.96	92.99	238.97
	$RMSE_O$ (m³/s)	20.09	23.83	20.59
	$RMSE_{aq}$ (m)	11.63	1.41	2.41
Validation	$RMSE_O$ (m³/s)	----	---	30.79
	$RMSE_{aq}$ (m)	---	---	1.21
	RMSE Bukan Dam storage (MCM)	---	---	78.47

The parameter set that minimizes Euclidean distance (Table 9) was subsequently used for a more detailed comparison against river discharge and GW level observations in the calibration period. Fig. 10.a shows scatter plots of monthly simulated vs observed streamflow during the calibration period for Nezamabad and Miyandoab hydrometric stations located on Zarineh Rood and Simineh Rood rivers, respectively. Fig. 10.b shows scatter plots of monthly simulated vs observed aquifer heads for all observation wells during the calibration period. The location of observation wells was shown in Fig. 10.c. Comparison between scatter plot with the 1:1 line shows good agreement between observed and simulated data with Nash-Sutcliffe Efficiency (*NSE*) values of 0.79 and 0.92, for

streamflow and GW levels, respectively. These values can be considered adequate (Moriasi et al., 2007). Fig. 10.c shows a map of the time-averaged RMSE for 39 observation wells used for the calibration period. This map shows no systematic trend in RMSE for these wells, indicating that spatial variation in aquifer heads is well reproduced by the model. Additional results with time-series of observed and simulated streamflow and aquifer heads for the calibration period are presented in Fig. S5.
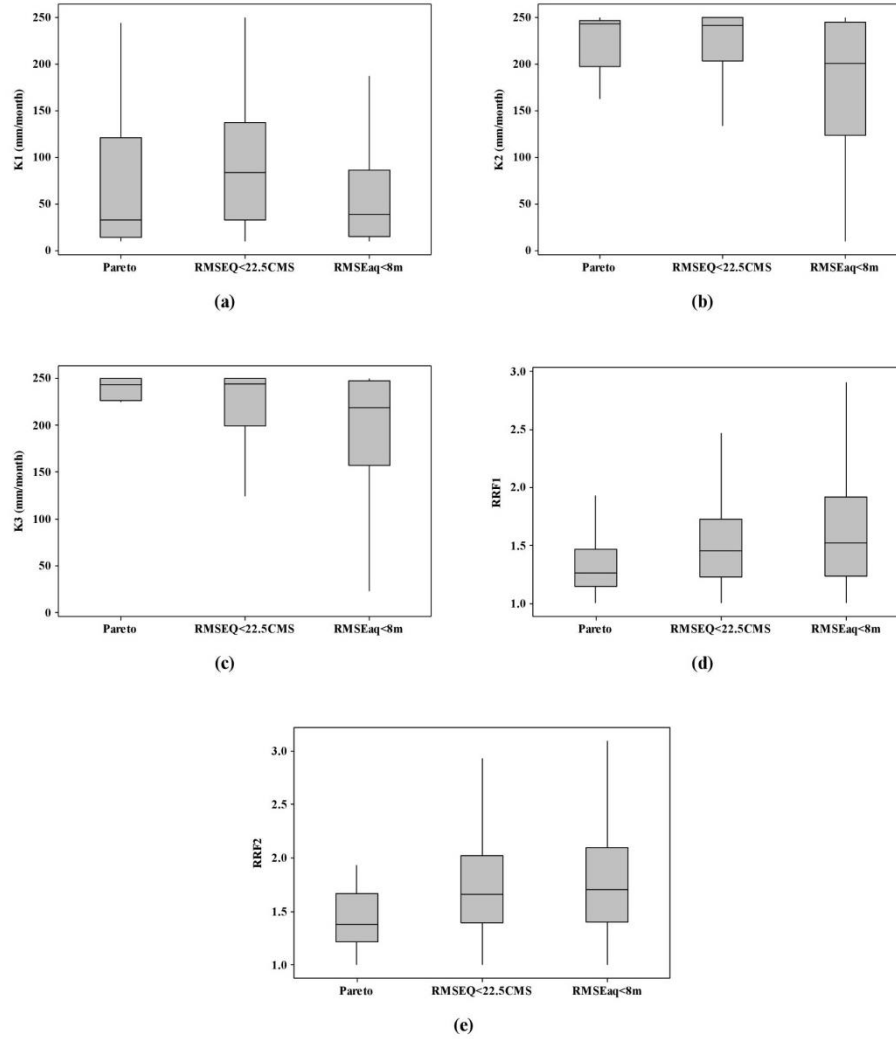

Fig. 9: Box plots of calibration parameters for three cases: parameter sets on the Pareto front, parameter sets for which $RMSE_Q$<22.5 m^3/s, and parameter sets for which $RMSE_{aq}$<8m (a. $K1$, b.$K2$, c. $K3$, d. $RRF1$, and e. $RRF2$)

Table 10: Correlation matrix of calibration parameters for a subset of simulations in the space of two objective functions by considering these criteria: $RMSE_Q$ <22.5 m^3/s and $RMSE_{aq}$<8m

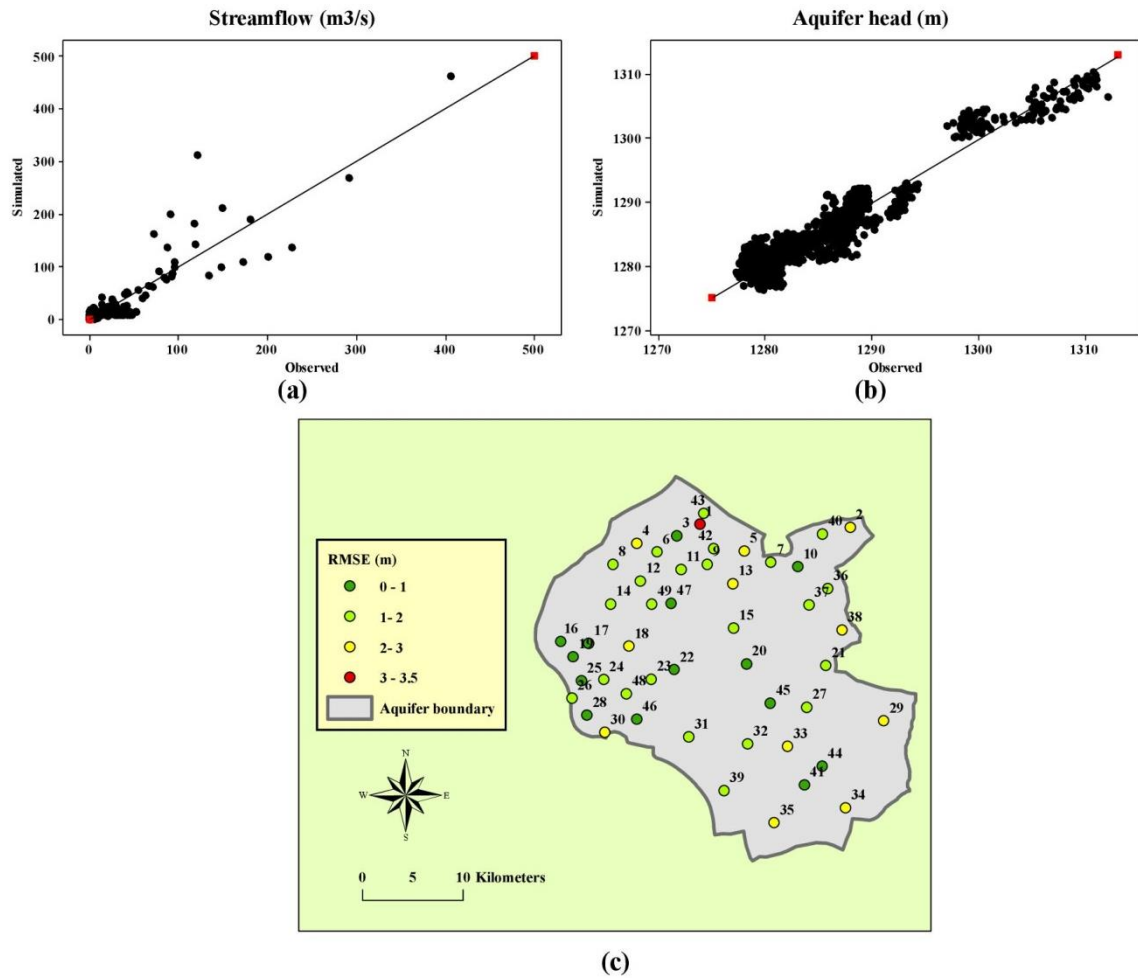|	RRF1	RRF2	K1	K2	K3
RRF1	1.00	-0.02	-0.13	0.10	0.01
RRF2	-0.02	1.00	0.13	0.13	0.09
K1	-0.13	0.13	1.00	0.15	0.26
K2	0.10	0.13	0.15	1.00	0.19
K3	0.01	0.09	0.26	0.19	1.00

Fig. 10: Calibration results: (a) Scatter plots of monthly simulated vs observed streamflow for Nezamabad and Miyandoab hydrometric stations, (b) Scatter plots of monthly simulated against observed aquifer heads for all observation wells during the calibration period, (c) Spatial variation in aquifer head RMSE for observation wells used in calibration and validation. Each observation well is identified by a number, with wells 1 to 39 corresponding to calibration wells and wells 40 to 49 corresponding to validation wells.

Fig. 11 presents observed and simulated streamflow and GW head for the validation period. Fig. 11.a present monthly time-series of observed and simulated streamflow of Nezamabad for the validation period (1991-2001). This figure shows that the model is able to simulate monthly dynamics in streamflow, with annual maxima occurring in April and May due to precipitation during these months (see Table S1). Fig. 11.b present monthly time-series of observed and simulated aquifer head for a validation well. This figure shows that the model mimics monthly variations in GW levels due to GW pumping for irrigation, which starts in April (high GW levels) and ends in October (low GW levels). Fig. 11.c shows monthly time-series of observed and simulated storage volume for Bukan dam in the period 1991-2013. The height of Bukan dam was increased in 2008. The storage volume of the dam before and after increasing the height is 650 and 808 MCM, respectively, and this change is visible in Fig. 11.c. The years 1999, 2000, 2001, and 2008 are extreme dry years in Miyandoab plain (see section 4.4). In these years, streamflow, GW levels, and storage volume of the Bukan dam were significantly decreased. Validation RMSE values for streamflow, GW levels, and Bukan dam storage in Table 9 confirm the adequate fit between observations and model simulations. Note that the RMSE value for the 10 validation wells is smaller than the RMSE value for the 39 calibration wells. More results about monthly time-series of observed and simulated streamflow and GW head for the validation period are presented in Fig. S6.
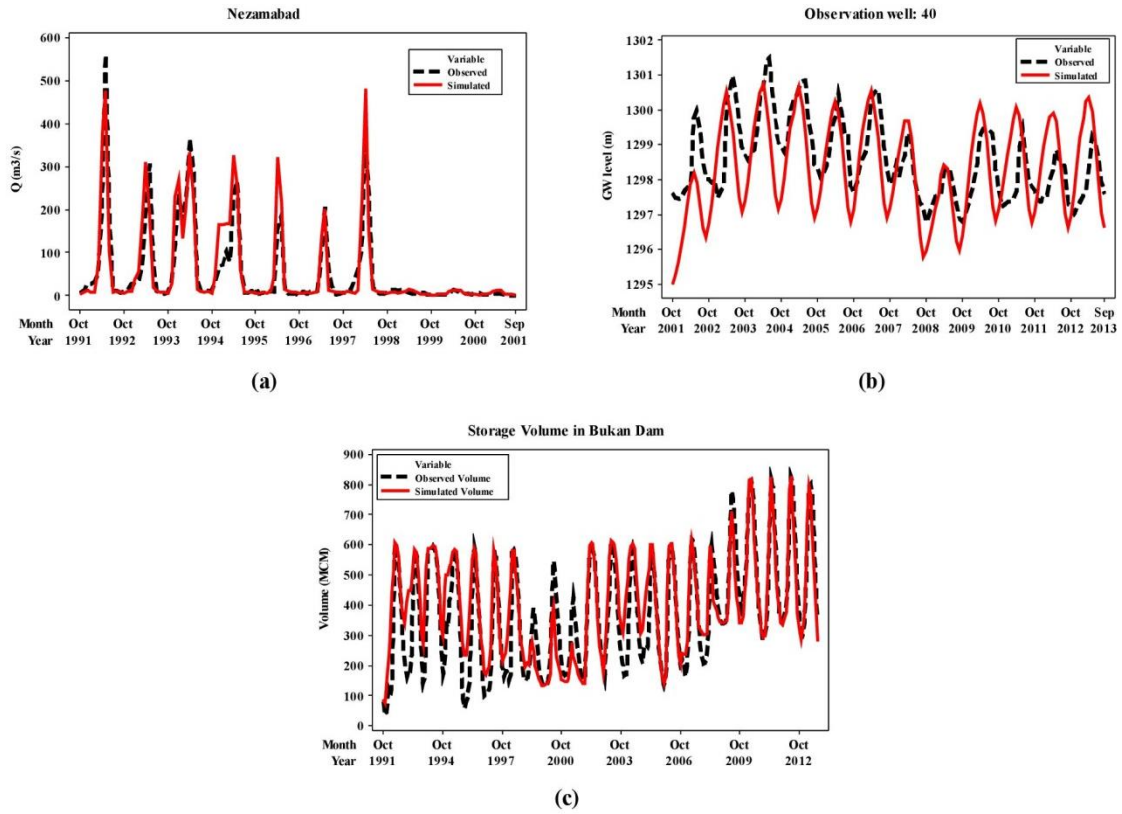
21

Fig. 11: Validation results: (a) Monthly time-series of observed and simulated streamflow of Nezamabad hydrometric station, (b) Monthly time-series of observed and simulated aquifer head for observation well 40, and (c) Monthly time-series of observed and simulated storage volume of Bukan dam

4.3. Calculated water balances

Fig. 12 shows the simulated time-averaged (2002-2013) annual water balance of the coupled SW-GW system, distinguishing between areas within (left in Figure) and outside (right) the Miyandoab aquifer boundary. According to the coupled system conceptualization and modeling, three sources of water inflow into the root zone within the Miyandoab aquifer boundary are SW extraction for irrigation (721.93 MCM), GW extraction for irrigation (124.80 MCM), and effective precipitation (172.26 MCM). Outflow from the root zone is composed of actual evapotranspiration (297.10 MCM), surface runoff (537.76 MCM), GW recharge (180.06 MCM), and storage change in the root zone (4.07 MCM). These results indicate that overall irrigation demand is supplied by 85% SW extraction and 15% GW extraction. Moreover, surface runoff is large and three times the amount of GW recharge. The monthly distribution of water balance components for the root zone within the Miyandoab aquifer boundary is presented in Table S14. Tables S15 and S16 show annual time-averaged (2002-2013) actual and potential ET in mm for orchards and crops in the root zone within the Miyandoab aquifer boundary, respectively. According to these tables, the ratio of actual to potential ET is between 70% and 80%.

Fig. 12 further shows three sources of water inflow into the root zone for the area outside of the Miyandoab aquifer boundary: SW extraction for irrigation (149.24 MCM), GW extraction for irrigation (179.68 MCM), and effective precipitation (96.05 MCM). Outflow from the root zone is composed of actual evapotranspiration (150.86 MCM), surface runoff and interflow (176.00 MCM), GW recharge (97.77 MCM), and storage change in the root zone (0.34 MCM). These results indicate that irrigation demand is supplied by 45% SW extraction and 55% GW extraction. Moreover, surface runoff is large and about two times the amount of GW recharge. The monthly distribution of water balance components for the root zone outside Miyandoab aquifer boundary is presented in Table S17. Tables S18 and S19 show annual time-averaged (2002-2013) actual and potential ET in mm for orchards and crops in the

22

external agricultural zones, respectively. According to these results, the ratio of actual to potential ET for agricultural zones outside the Miyandoab aquifer boundary is between 60% and 80%.
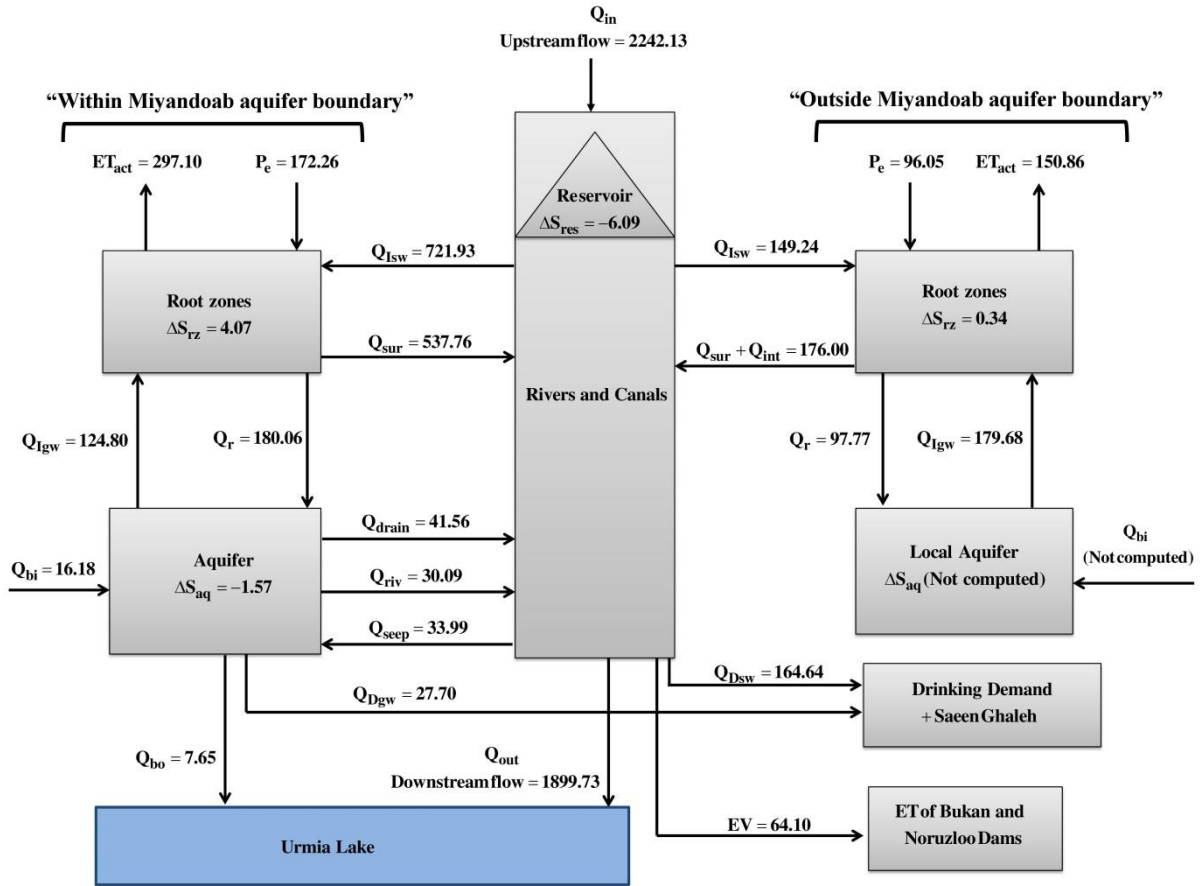

Fig 12: Simulated water balance components for the coupled SW-GW system of the Miyandoab plain. Each number is an average over the period 2002-2013 and is expressed in MCM/year. Variables are defined in Tables 1-4.

Referring to the aquifer water balance in Fig. 12, the inflows include, in order of importance, GW recharge from irrigation and precipitation (180.06 MCM), seepage from rivers (33.99 MCM), and lateral GW inflows (16.18 MCM). Aquifer outflows, in order of importance, are GW extraction for irrigation and drinking demand (152.5 MCM), GW discharge to drains (41.56 MCM), GW discharge to rivers (30.09 MCM), and lateral GW outflows (7.65 MCM). On average over the period 2002-2013, total inflow into Miyandoab aquifer is 230.23 MCM and total outflow is 231.80 MCM, resulting in a small reduction in GW storage (-1.57 MCM). Hence, even though long-term recharge is larger than GW extraction (pumping), aquifer storage is declining in the long-term, underscoring the importance of accounting for SW-GW interactions and of not only considering recharge and pumping when evaluating sustainability of GW use (Bredehoeft, 2002). Table S20 presents simulated time-averaged (2001-2013) annual and monthly water balance components of the Miyandoab aquifer. This table indicates that change of GW storage in the Miyandoab aquifer is positive from October to April and negative from May to September. Table S13 shows that computed water balance components for the GW system are similar to those from other studies.

Finally, the lumped water balance of all reservoirs, rivers and canals consists of the following inflows: upstream inflow into rivers (2242.13 MCM), surface runoff and interflow (713.76 MCM), GW discharge to rivers (30.09 MCM), and GW drainage (41.56 MCM). The amounts of GW discharge to rivers and GW drainage are small compared to upstream inflow and to surface runoff and interflow. Outflows include discharge to Urmia lake (1899.73 MCM), SW extraction for agriculture (871.17), SW extraction for drinking and Saeen Ghaleh (164.64

MCM), evaporation from Bukan storage dam and Norouzlou diversion dam (64.10 MCM), and seepage from rivers (33.99 MCM). Therefore, the most important outflows are discharge to Urmia Lake and SW extraction for irrigation. In summary, total inflow into reservoir, rivers and canals is 3027.54 MCM, total outflow is 3033.63 MCM, and total storage (basically, storage in Bukan dam) has declined slightly (-6.09 MCM). Table S21 presents time-averaged (2001-2013) monthly and annual water balance components for reservoir, rivers and canals. This table indicates that storage change in Bukan storage dam is positive from October to April and negative from May to September. Calculated time-averaged water balance components of the SW system (Table S22) are similar to those reported in a previous study by the Ministry of Energy of Iran (Ministry of Energy of Iran, 2016). Moreover, Table S23 presents ET actual, total water use for irrigation, and irrigation efficiency of our study and from a previous Ministry of Energy study. The irrigation efficiency is the ratio of the ET actual to the total water extraction for irrigation. According to this Table, the irrigation efficiency in the Miyandoab Plain is 38%. The main irrigation method in the region is basin irrigation, which contributes to this fairly small irrigation efficiency Irrigation efficiency of basin irrigation changes between 30% to 60% (Bos and Nugteren, 1990), and an overall irrigation efficiency of 40% is not unusual (Brouwer et al., 2001).

4.4. Quantification of historical drought impacts in Miyandoab plain

In this final section, we use the calibrated SW-GW model to analyze behavior of the Miyandoab plain hydrological system during dry years in the historical record. Fig. 13.a shows observed annual precipitation during 1992- 2013. Dry years include 1999, 2000, 2001, and 2008. For these years, precipitation was 40% smaller than the average during 2002-2013. The resulting reductions in SW supply (upstream river discharge) directly affect two competing goals in this region: sustaining agricultural production in Miyandoab plain and maintaining downstream discharge into Lake Urmia.

Drought impacts on agricultural production and the subsurface water system (root zone, aquifer)

Crop water supply during dry years changed relative to average conditions in 2002-2013: there was a 40% decrease in effective precipitation, a 9% reduction in SW extraction for irrigation, and a 3% increase in GW extraction for irrigation. Hence, GW extraction only partially compensated for the decrease in SW supply, resulting in a reduction in simulated crop ET (and yield), as shown by the annual time series of simulated ratio of actual to potential ET in Fig. 13d and the map in Fig. 14. These results illustrate that crop production in Miyandoab plain is sensitive to water supply reductions during droughts. While reductions in SW supply can in principle be managed by corresponding increases in GW pumping, average simulated pumping during dry years was near full capacity (96%), indicating that current pumping capacities in the region are not sufficient to satisfy irrigation water demand during dry years. Whether increasing pumping capacity in the region is a sustainable option for safeguarding crop production during droughts, depends on the impact of increased GW pumping on GW flows and levels. Fig. 15 shows how the simulated aquifer water balance changes during dry years: GW recharge decreased by 10% compared to 2002-2013, river seepage decreased by 61%, GW extraction increased by 3%, GW discharge to rivers decreased by 12%, and GW discharge to drains decreased by 37%. Overall, total inflow into Miyandoab aquifer decreased by 17% (relative to average conditions), total outflow decreased by 6%, and GW storage decreased by 26.98 MCM in dry years. While this storage reduction may seem fairly small, the effect on GW levels is relatively pronounced due to the small specific yield of the Miyandoab aquifer (on average about 0.035, see Fig. 6b). Fig. 13b

shows significant drops in observed and simulated GW levels during dry years (1999-2001 and 2008-2009). Note that the observed GW hydrograph was taken from the official report for 2001-2011 (Ministry of Energy of Iran, 2014) and was calculated using the weighted average of observation wells. The simulated hydrograph in Fig. 13b, on the other hand, was calculated by averaging simulated GW levels over the entire aquifer. Therefore, observed and simulated time-series are not expected to match exactly, although it is clear from Fig. 13b that the model captures the same dynamics as the data. Fig. 16 shows that changes in GW level during dry years are not spatially uniform but are concentrated in zones Z1, Z2, Z3, Z6, Z7, Z8, and Z9-4. The map of simulated GW levels is presented in Fig. S7.
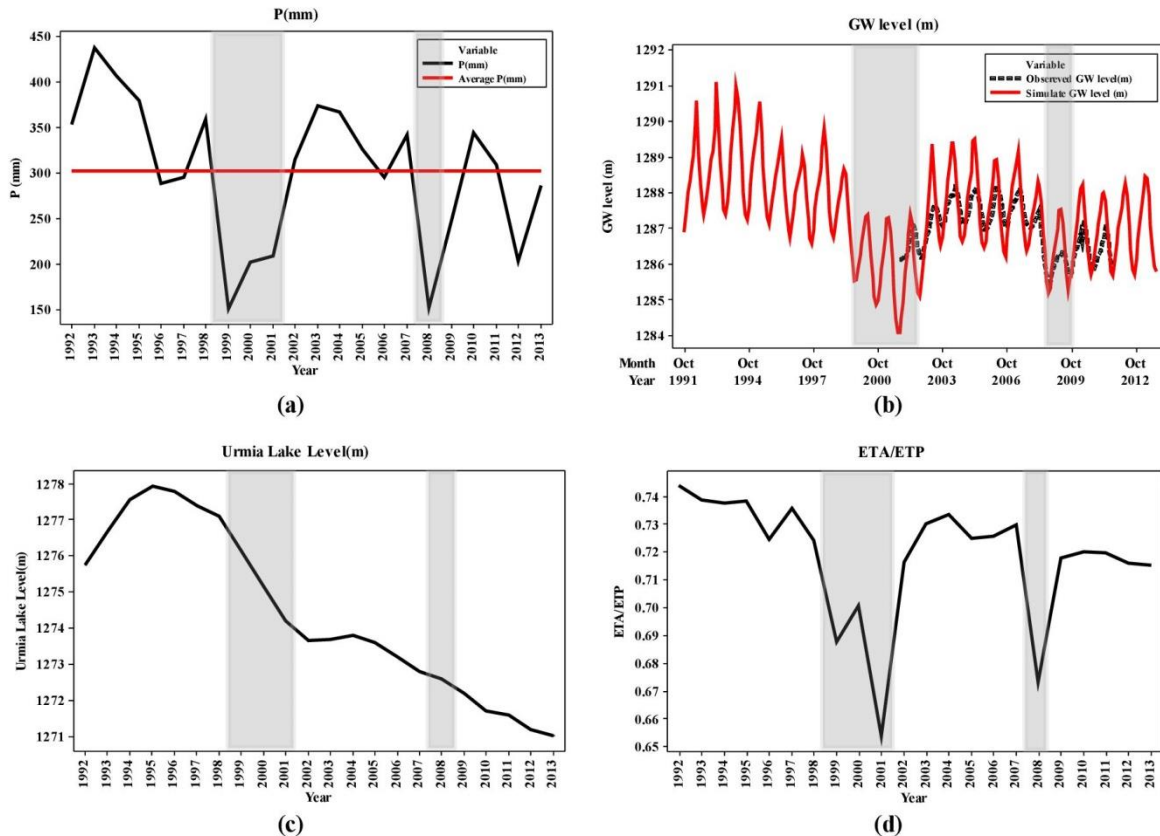

Fig. 13: Drought impacts on the SW-GW system of the Miyandoab plain: (a) Annual time series of observed precipitation, (b) Monthly time series of simulated and observed GW levels, (c) Annual time series of observed water levels of Urmia lake, and (d) Annual time series of the simulated ratio of actual to potential crop ET (Dry years are indicated by shaded boxes)

Drought impacts on Lake Urmia and the surface water system (rivers, canals, reservoirs)

Fig. 15 shows a 61% reduction in upstream river inflow in dry years compared to 2002-2013. This is accompanied by a 14% reduction in interflow and surface runoff, a 12% decrease in GW discharge to rivers, and a 37% reduction in GW Drainage. Downstream river discharge into Urmia lake is also significantly reduced (64% decrease), as are SW extraction for agriculture (9% decrease), river seepage (61% decrease), drinking demands and Saeen Ghaleh demand (42% decrease), and reservoir evaporation (33% decrease). Overall, total inflow into reservoirs, rivers and canals decreased by 49% compared to average conditions, total outflow decreased by 46%, and storage in Bukan storage dam decreased by 77.34 MCM during dry years. The decrease in downstream river discharge in Zarrineh Rood and Simineh Rood, which accounts for 50% of total annual inflow into Urmia Lake, had important consequences for lake water levels. Fig. 13c shows that lake water levels have been decreasing since 1995, and the extent of the lake has consequently shrunk significantly. Dried up parts of Urmia Lake have been transformed into saline areas that contain industrial pollutants, pesticides, and heavy metals, leading to wind-blown pollution that

25

affects ecosystems, agriculture, and livelihoods of surrounding areas (Hassanzadeh et al., 2012). The Iranian government has established the Urmia Lake Restoration Program to save Urmia Lake and its surroundings. This program evaluates restoration measures under various climatic, socioeconomic and management scenarios (Shadkam et al., 2016). The SW-GW model developed here is a valuable tool for evaluating water balance impacts (e.g. changes in runoff and recharge) in Miyandoab plain of proposed measures using various management scenarios of the Urmia Lake Restoration Program. Our calibrated model is capable of capturing observed hydrological dynamics and accounts for important SW-GW interactions in the region.
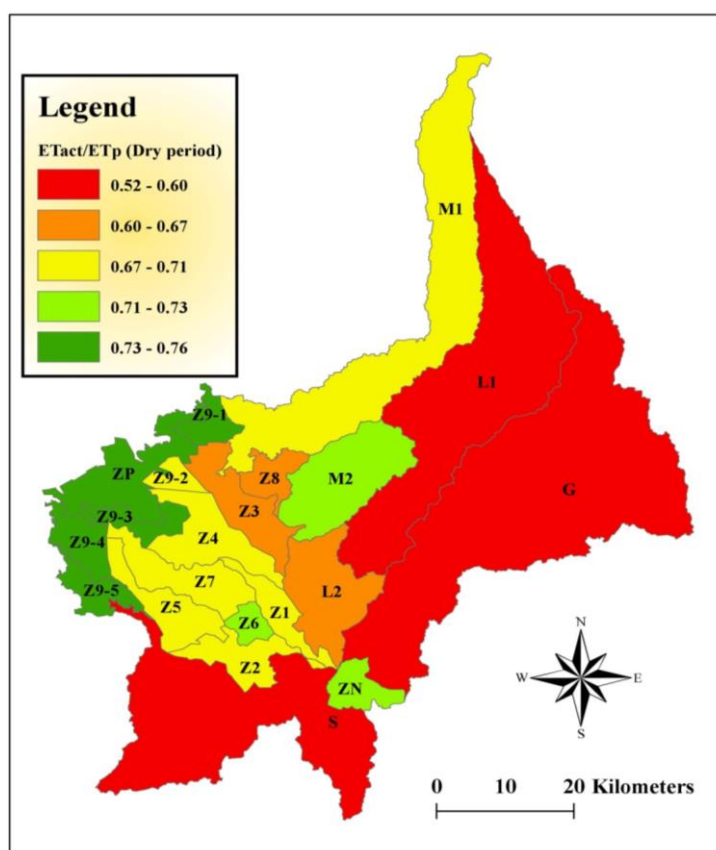

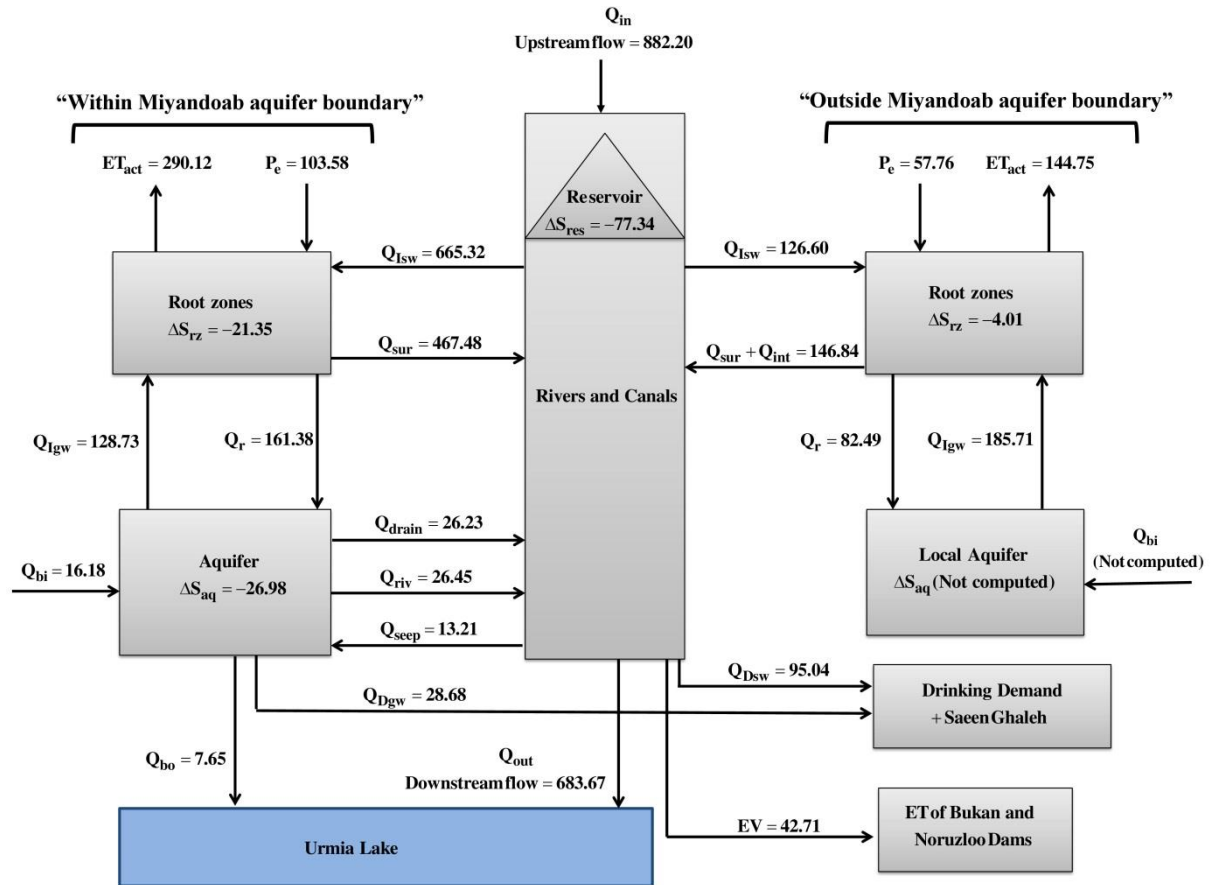**Fig. 14: Simulated ratio of actual to potential ET during dry years**

Fig. 15: Simulated water balance components for the coupled SW-GW system of the Miyandoab plain. Each number is an average for four historically dry years (1999, 2000, 2001, and 2008) and is expressed in MCM/year. Variables are defined in Tables 1-4.
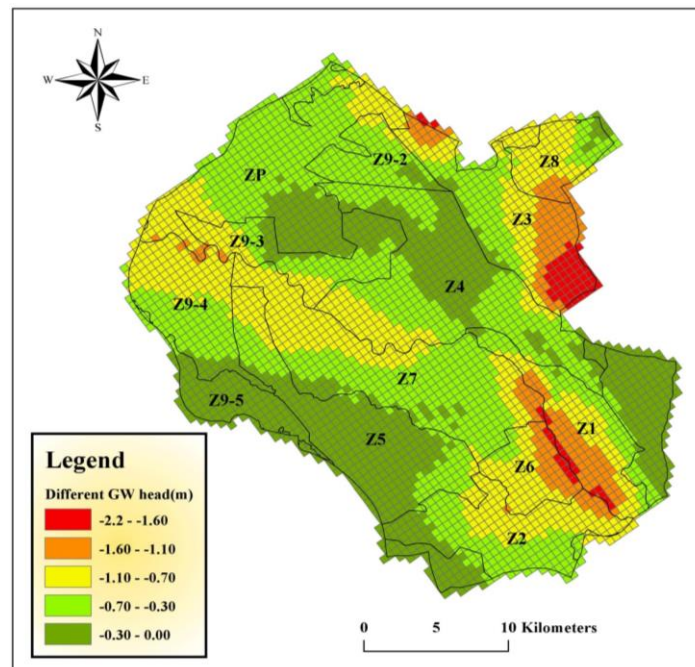

Fig. 16: Changes in simulated GW levels during dry years vs. average years

5. Conclusions

This study developed and applied the first coupled SW-GW flow model for the irrigated Miyandoab plain located in the Urmia basin, in the northwest of Iran. This plain is a strategic irrigated area in the Urmia basin with significant SW-GW interactions and strong impacts of irrigated agriculture. Safeguarding downstream environmental flows is an important water management issue in this region, due to the shrinking of Lake Urmia, located downstream of the agricultural plain. Moreover, based on the observed hydrograph of the Miyandoab aquifer, GW head has dropped over time due to a reduction of precipitation as well as an increase of GW withdrawal for agricultural purposes.

The hydrological model includes SW (rivers, canals, and reservoir), root-zone soil moisture, and GW components, which are implemented using a dynamic coupling between MODFLOW and WEAP. This paper focuses on the root-zone water balance model to keep track of dynamic changes in soil moisture and simultaneously calculates irrigation demand, GW recharge, evapotranspiration, interflow, and surface runoff. In addition, the MOPSO algorithm is used for multi-objective calibration of the WEAP-MODFLOW model parameters using GW level and river discharge data. Calibration results show relatively little trade-off between matching the two objective functions, i.e. RMSE of GW levels ($RMSE_{aq}$) and river discharge ($RMSE_Q$), and (ii) accurate simulation of historical conditions with $RMSE_{aq}$ ($RMSE_Q$) equal to 2.41 m (20.59 m^3/s) and 1.21 m (30.79 m3/s) for resp. calibration and validation periods. These results indicate that the various model components, including WEAP's soil moisture method, which is used here for calculating root-zone processes, provide an adequate representation of the SW-GW hydrology of the region. It is further shown that calibration using the two data sources (GW levels and river discharge) leads to better constrained parameters compared to using either data source alone.

The calibrated (and validated) model was subsequently applied to generate new quantitative insights of historical drought impacts in the Miyandoab plain. During historically dry years, precipitation decreased by 40% and this change affected the water balance components in the SW-GW system of the Miyandoab plain. Simulation results show that total inflow and outflow of Miyandoab aquifer decreased by 17% and 6%, respectively, during dry years (compared to average conditions), and that both simulated and observed GW head dropped in response. Moreover, the upstream flow of rivers decreased by 61% and the discharge to Urmia Lake decreased by 64% in dry years relative to average conditions. Model simulations further provide two important insights for future water management in the region, namely that crop water demand cannot be met during droughts due to limited GW pumping capacity, and that increased GW pumping has a relatively strong impact on GW levels due to the small specific yield of the aquifer. The SW-GW model developed here is a valuable tool for evaluating water balance impacts in Miyandoab plain of proposed measures using various management scenarios of the Urmia Lake Restoration Program. Our calibrated model is capable of capturing observed hydrological dynamics and accounts for important SW-GW interactions in the region.

Competing interests

The authors declare no competing interests.

References

Afshar, A., Shojaei, N., Sagharjooghifarahani, M., 2013. Multiobjective Calibration of Reservoir Water Quality Modeling Using Multiobjective Particle Swarm Optimization (MOPSO). Water Resour. Manag. 27, 1931–1947. https://doi.org/10.1007/s11269-013-0263-x

Ahmadzadeh, H., Morid, S., Delavar, M., Srinivasan, R., 2016. Using the SWAT model to assess the impacts of changing irrigation from surface to pressurized systems on water productivity and water saving in the Zarrineh Rud catchment. Agric. Water Manag. 175, 15–28. https://doi.org/10.1016/j.agwat.2015.10.026

Alizadeh, H., Mousavi, S.J., 2013. Coupled stochastic soil moisture simulation-optimization model of deficit irrigation. Water Resour. Res. 49, 4100–4113. https://doi.org/10.1002/wrcr.20282

Arnold, J.G., Srinivasan, R., Muttiah, R.S., Williams, J.R., 1998. Large area hydrologic modeling and assessment part I: Model development. J. Am. Water Resour. Assoc. 34, 73–89. https://doi.org/10.1111/j.1752-1688.1998.tb05961.x

Bos, M.G., Nugteren, J., 1990. On irrigation efficiencies. 4th edition.

Bredehoeft, J.D., 2002. The water budget myth revisited: Why hydrogeologists model. Ground Water 40, 340–345. https://doi.org/10.1111/j.1745-6584.2002.tb02511.x

Brouwer, C., Prins, K., Heibloem, M., 2001. Irrigation Water Management: Irrigation Scheduling. fao.org 66.

Buras, N., 1963. Conjunctive Operation of Dams and Aquifers. J. Hydraul. Div. 89, 111–131.

Chávez-Morales, J., Mariño, M.A., Holzapfel, E.A., 1992. Planning Simulation Model of Irrigation District. J. Irrig. Drain. Eng. 118, 74–87. https://doi.org/10.1061/(asce)0733-9437(1992)118:1(74)

Clarke, D., Smith, M., El-Askari, K., 1998. CropWat for Windows: User Guide. IHE.

Coello, C.A.C., Pulido, G.T., Lechuga, M.S., 2004. Handling Multiple Objectives With Particle Swarm Optimization. IEEE Trans. Evol. Comput. 8, 256–279. https://doi.org/https://ieeexplore.ieee.org/document/1304847

Doherty, J., 2003. Ground water model calibration using pilot points and regularization. Ground Water 41, 170–177. https://doi.org/10.1111/j.1745-6584.2003.tb02580.x

Droubi, A., Al-Sibai, M., Abdallah, A., Wolfer, J., Huber, M., Hennings, V., El Hajji, K., Dechiech, M., 2008a. Management, Protection and Sustainable Use of Groundwater and Soil Resources in the Arab Region. Development and Application of a Decision Support System (DSS) for Water Resources Management in Zabadani Basin, SYRIA and Berrechid Basin, MOROCCO, Evaluation.

Droubi, A., Al-Sibai, M., Abdallah, A., Zahra, S., Obeissi, M., Wolfer, J., Huber, M., Hennings, V., Schelkes, K., 2008b. A Decision Support System (DSS) for Water Resources Management, – Design and Results from a Pilot Study in Syria, in: Climatic Changes and Water Resources in the Middle East and North Africa. pp. 199–225. https://doi.org/10.1007/978-3-540-85047-2_16

Ehtiat, M., Jamshid Mousavi, S., Srinivasan, R., 2018. Groundwater Modeling Under Variable Operating Conditions Using SWAT, MODFLOW and MT3DMS: a Catchment Scale Approach to Water Resources Management. Water Resour. Manag. 32, 1631–1649. https://doi.org/10.1007/s11269-017-1895-z

FAO, 1980. Drainage Design Factors. FAO Irrigation and Drainage Paper No. 38., Rome.

Fredericks, J.W., Labadie, J.W., Altenhofen, J.M., 1998. Decision Support System for Conjunctive Stream-Aquifer Management. J. Water Resour. Plan. Manag. 124, 69–78. https://doi.org/10.1061/(asce)0733-9496(1998)124:2(69)

Galaitsi, S., 2018. WEAP: Water Evaluation And Planning System [WWW Document]. URL https://www.weap21.org/index.asp?action=9&read=3587&fID=30 (accessed 6.18.19).

Ghaheri, M., Baghal-Vayjooee, M.H., Naziri, J., 1999. Lake Urmia, Iran: A summary review. Int. J. Salt Lake Res. 8, 19–22. https://doi.org/10.1023/A:1009062005606

Hadded, R., Nouiri, I., Alshihabi, O., Maßmann, J., Huber, M., Laghouane, A., Yahiaoui, H., Tarhouni, J., 2013. A Decision Support System to Manage the Groundwater of the Zeuss Koutine Aquifer Using the WEAP-MODFLOW Framework. Water Resour. Manag. 27, 1981–2000. https://doi.org/10.1007/s11269-013-0266-7

Hamzehkhani, H., Aghaie, M.M., Tajrishi, M., 2015. Miyandoab plain Groundwater modelling with the use of remote sensing technology to assess the impact of changes in aquifer conditions on surface flow., Technical

report of Urmia Lake Restoration National Committee (ULRNC) & Sharif University of Technology Remote Sensing Research Center (available in Persian).

Harbaugh, A.W., 2005. MODFLOW-2005, the US Geological Survey modular ground-water model: the ground-water flow process. US Department of the Interior, US Geological Survey.

Hassanzadeh, E., Zarghami, M., Hassanzadeh, Y., 2012. Determining the Main Factors in Declining the Urmia Lake Level by Using System Dynamics Modeling. Water Resour. Manag. 26, 129–145. https://doi.org/10.1007/s11269-011-9909-8

Hesami, A., Amini, A., 2016. Changes in irrigated land and agricultural water use in the Lake Urmia basin. Lake Reserv. Manag. 32, 288–296. https://doi.org/10.1080/10402381.2016.1211202

Höllermann, B., Giertz, S., Diekkrüger, B., 2010. Benin 2025-Balancing Future Water Availability and Demand Using the WEAP "Water Evaluation and Planning" System. Water Resour. Manag. 24, 3591–3613. https://doi.org/10.1007/s11269-010-9622-z

Huntington, J.L., Niswonger, R.G., 2012. Role of surface-water and groundwater interactions on projected summertime streamflow in snow dominated regions: An integrated modeling approach. Water Resour. Res. 48. https://doi.org/10.1029/2012WR012319

Ingol-Blanco, E., McKinney, D.C., 2012. Development of a Hydrological Model for the Rio Conchos Basin. J. Hydrol. Eng. 18, 340–351. https://doi.org/10.1061/(asce)he.1943-5584.0000607

Le Page, M., Berjamy, B., Fakir, Y., Bourgin, F., Jarlan, L., Abourida, A., Benrhanem, M., Jacob, G., Huber, M., Sghrer, F., Simonneaux, V., Chehbouni, G., 2012. An Integrated DSS for Groundwater Management Based on Remote Sensing. The Case of a Semi-arid Aquifer in Morocco. Water Resour. Manag. 26, 3209–3230. https://doi.org/10.1007/s11269-012-0068-3

Leavesley, G.H., Lichty, R.W., Troutman, B.M., Saindon, L.G., 1983. Precipitation-runoff modeling system (PRMS)-User's Manual. U.S. Geological Survey, Washington.

Mancosu, N., Snyder, R.L., Kyriakakis, G., Spano, D., 2015. Water scarcity and future challenges for food production. Water (Switzerland) 7, 975–992. https://doi.org/10.3390/w7030975

Markstrom, S.L., Niswonger, R.G., Regan, R.S., Prudic, D.E., Barlow, P.M., 2008. GSFLOW—Coupled Ground-Water and Surface-Water Flow Model Based on the Integration of the Precipitation-Runoff Modeling System (PRMS) and the Modular Ground-Water Flow Model (MODFLOW-2005), Geological Survey (US). https://doi.org/10.13140/2.1.2741.9202

Ministry of Energy of Iran, 2016. Implementation strategies for 40% reduction of Agricultural Water Consumption in Zarrineh Roud and Simineh rood River basins, Vol. 7: Planning and management studies of water resources and consumption in Miyandoab plain (available in Persian).

Ministry of Energy of Iran, 2014. Studies on updating the water resources balance in the Urmia Lake basin (available in Persian).

Mohammadpour, M., Bagheri, A., 2017. Common pool water resources management considering a regulator interference: A game theory approach to derive managerial policies for Urmia lake, Iran. Lakes Reserv. Res. Manag. 22, 85–94. https://doi.org/10.1111/lre.12158

Montazar, A., Riazi, H., Behbahani, S.M., 2010. Conjunctive water use planning in an irrigation command area. Water Resour. Manag. 24, 577–596. https://doi.org/10.1007/s11269-009-9460-z

Moriasi, D.N., Arnold, J.G., Van Liew, M.W., Bingner, R.L., Harmel, R.D., Veith, T.L., 2007. Curriculum for the Academy Profession Degree Programme in Multimedia Design and Communication - National part, 2017. Am. Soc. Agric. Biol. Eng. 50, 885–900. https://doi.org/10.13031/2013.23153

Moussa, R., Chahinian, N., 2009. Comparison of different multi-objective calibration criteria using a conceptual rainfall-runoff model of flood events. Hydrol. Earth Syst. Sci. 13, 519–535. https://doi.org/10.5194/hess-13-519-2009

Nash, J.E., Sutcliffe, J. V., 1970. River flow forecasting through conceptual models part I - A discussion of principles. J. Hydrol. 10, 282–290. https://doi.org/10.1016/0022-1694(70)90255-6

Nouiri, I., Yitayew, M., Maßmann, J., Tarhouni, J., 2015. Multi-objective Optimization Tool for Integrated Groundwater Management. Water Resour. Manag. 29, 5353–5375. https://doi.org/10.1007/s11269-015-1122-

Paydar, Z., Qureshi, M.E., 2012. Irrigation water management in uncertain conditions-Application of modern portfolio theory. Agric. Water Manag. 115, 47–54. https://doi.org/10.1016/j.agwat.2012.08.004

Raskina, P., Hansen, E., Zhu, Z., Stavisky, D., 1992. Simulation of water supply and demand in the aral sea region. Water Int. 17, 55–67. https://doi.org/10.1080/02508069208686127

Rodriguez, L.B., Cello, P.A., Vionnet, C.A., Goodrich, D., 2008. Fully conservative coupling of HEC-RAS with MODFLOW to simulate stream-aquifer interactions in a drainage basin. J. Hydrol. 353, 129–142. https://doi.org/10.1016/j.jhydrol.2008.02.002

Rogers, P., Smith, D. V., 1970. The Integrated Use of Ground and Surface Water in Irrigation Project Planning. Am. J. Agric. Econ. 52, 13–24. https://doi.org/10.2307/1238158

Rossman, L.A., 2004. Storm water management model user manual. Version 5. National Risk Management Research Laboratory, Office of Research and Development, US Environmental Protection Agency.

Rousta, B.A., Araghinejad, S., 2015. Development of a Multi Criteria Decision Making Tool for a Water Resources Decision Support System. Water Resour. Manag. 29, 5713–5727. https://doi.org/10.1007/s11269-015-1142-4

Safavi, H.R., Esmikhani, M., 2013. Conjunctive Use of Surface Water and Groundwater: Application of Support Vector Machines (SVMs) and Genetic Algorithms. Water Resour. Manag. 27, 2623–2644. https://doi.org/10.1007/s11269-013-0307-2

Sala, S., Formentin, G., Porro, A., 2015. Technical perspective of ICT as a tool for improved responsible management of the Orontes Basin. Sci. Dipl. Transbound. water Manag. Orontes River case.

Schoups, G., Addams, C.L., Gorelick, S.M., 2005. Multi-objective calibration of a surface water-groundwater flow model in an irrigated agricultural region: Yaqui Valley, Sonora, Mexico. Hydrol. Earth Syst. Sci. 9, 549–568. https://doi.org/10.5194/hess-9-549-2005

Schoups, G., Addams, C.L., Minjares, J.L., Gorelick, S.M., 2006. Sustainable conjunctive water management in irrigated agriculture: Model formulation and application to the Yaqui Valley, Mexico. Water Resour. Res. 42. https://doi.org/10.1029/2006WR004922

Shadkam, S., Ludwig, F., van Vliet, M.T., Pastor, A., Kabat, P., 2016. Preserving the world second largest hypersaline lake under future irrigation and climate change. Sci. Total Environ. 559, 317–325. https://doi.org/10.1016/j.scitotenv.2016.03.190

Sieber, J., Purkey, D., 2015. WEAP Water Evaluation and Planning System: User Guide, Stockholm Environment Institute, US Center.

Singh, A., 2014a. Conjunctive use of water resources for sustainable irrigated agriculture. J. Hydrol. 519, 1688–1697. https://doi.org/10.1016/J.JHYDROL.2014.09.049

Singh, A., 2014b. Simulation-optimization modeling for conjunctive water use management. Agric. Water Manag. 141, 23–29. https://doi.org/10.1016/j.agwat.2014.04.003

Sophocleous, M.A., Koelliker, J.K., Govindaraju, R.S., Birdie, T., Ramireddygari, S.R., Perkins, S.P., 1999. Integrated numerical modeling for basin-wide water management: The case of the Rattlesnake Creek basin in south-central Kansas. J. Hydrol. 214, 179–196. https://doi.org/10.1016/S0022-1694(98)00289-3

Tang, Y., Reed, P., Wagener, T., 2006. How effective and efficient are multiobjective evolutionary algorithms at hydrologic model calibration? Hydrol. Earth Syst. Sci. 10, 289–307. https://doi.org/10.5194/hess-10-289-2006

Tehrani, M.V., Bagheri, A., Monem, M.J., Khan, S., 2012. Analysing structural and non-structural options to improve utility of irrigation areas using a system dynamics approach. Irrig. Drain. 61, 604–621. https://doi.org/10.1002/ird.1697

Tian, Y., Zheng, Y., Wu, B., Wu, X., Liu, J., Zheng, C., 2015. Modeling surface water-groundwater interaction in arid and semi-arid regions with intensive agriculture. Environ. Model. Softw. 63, 170–184. https://doi.org/10.1016/j.envsoft.2014.10.011

Wolfer, J., 2009a. Management and Protection and Sustainable Use of Groundwater and Soil Resources in the Arab Region. Technical Paper on MODFLOW2000 constraints for preparing/ modifying a groundwater flow model to be linked to WEAP.

Wolfer, J., 2009b. Management and Protection and Sustainable Use of Groundwater and Soil Resources in the Arab Region. Technical Paper on Groundwater Recharge/ Surface Runoff Entry Options in WEAP.

Yates, D., Sieber, J., Purkey, D., Huber-Lee, A., 2005. WEAP21 - A demand-, priority-, and preference-driven water planning model. Part 1: Model characteristics. Water Int. 30, 487–500. https://doi.org/10.1080/02508060508691893

Zheng, C., Wang, P.P., 1999. MT3DMS: A modular three-dimensional multispecies model for simulation of advection, dispersion and chemical reactions of contaminants in groundwater systems, Documentation and User's Guide, Alabama University.